**Voltage-dependent activation of Rac1 by $Na_v1.5$ channels promotes cell migration**

**Running title:** Voltage-dependent migration via $Na_v1.5$ and Rac1

Ming Yang[1], Andrew D. James[1,2], Rakesh Suman[3], Richard Kasprowicz[3], Michaela Nelson[1,2], Peter J. O'Toole[4] and William J. Brackenbury[1,2*]

[1]Department of Biology, University of York, Heslington, York, YO10 5DD, UK

[2]York Biomedical Research Institute, University of York, Heslington, York, YO10 5DD, UK

[3]Phase Focus Ltd, Electric Works, Sheffield Digital Campus, Sheffield, S1 2BJ, UK

[4]Bioscience Technology Facility, Department of Biology, University of York, Heslington, York, YO10 5DD, UK

*Corresponding author:

Dr. William J. Brackenbury, Department of Biology and York Biomedical Research Institute, University of York, Heslington, York YO10 5DD, UK

Email: william.brackenbury@york.ac.uk

Tel: +44 1904 328284

Fax: +44 1904 328505

ORCID: 0000-0001-6882-3351

**Acknowledgements**

This work was supported by the Medical Research Council [G1000508], Cancer Research UK [A25922] and a Radhika V Sreedhar Scholarship.

**Data availability statement**

The data that support the findings of this study are available from the corresponding author upon reasonable request.

**Abstract**

Ion channels can regulate the plasma membrane potential ($V_m$) and cell migration as a result of altered ion flux. However, the mechanism by which $V_m$ regulates motility remains unclear. Here, we show that the $Na_v1.5$ sodium channel carries persistent inward $Na^+$ current which depolarizes the resting $V_m$ at the timescale of minutes. This $Na_v1.5$-dependent $V_m$ depolarization increases Rac1 colocalization with phosphatidylserine, to which it is anchored at the leading edge of migrating cells, promoting Rac1 activation. A genetically-encoded FRET biosensor of Rac1 activation shows that depolarization-induced Rac1 activation results in acquisition of a motile phenotype. By identifying $Na_v1.5$-mediated $V_m$ depolarization as a regulator of Rac1 activation, we link ionic and electrical signaling at the plasma membrane to small GTPase-dependent cytoskeletal reorganization and cellular migration. We uncover a novel and unexpected mechanism for Rac1 activation, which fine tunes cell migration in response to ionic and/or electric field changes in the local microenvironment.

**Keywords:** Breast cancer / membrane potential / migration / $Na_v1.5$ / Rac1

## Introduction

Cellular morphological changes and migration play key roles in normal physiological processes, including during embryonic development and tissue repair. On the other hand, dysfunctional migration occurs in many disease processes, including cancer metastasis (Bravo-Cordero, Hodgson, & Condeelis, 2012). In particular, mesenchymal migration, which is dependent on polarization and formation of lamellipodial protrusions at the leading edge of cells, enables carcinoma cells to escape from primary tumors into surrounding tissues (Friedl, Locker, Sahai, & Segall, 2012).

Dynamic and adaptable changes in actin polymerization lead to altered stiffness, elongation and branching, which in turn permits acquisition of a mesenchymal phenotype and formation of lamellipodial protrusions (Krause & Gautreau, 2014). These changes are tightly regulated by a multiplicity of signaling mechanisms which are coordinated by the Rho family of small GTPases (Ridley, 2015). One of the best studied Rho GTPases, Rac1, plays a critical role in regulating lamellipodia formation and migration (Wu et al., 2009). Rac1 cycles between active (GTP-bound) and inactive (GDP-bound) forms, catalyzed by guanine nucleotide exchange factors (GEFs) and GTPase-activating proteins (GAPs), respectively (Marei & Malliri, 2017). Rac1 translocates between cytoplasmic and plasma membrane-bound compartments, with activation predominantly occurring at the plasma membrane (Garcia-Mata, Boulter, & Burridge, 2011). Translocation of Rac1 to the plasma membrane and interaction with phospholipids precede interaction with GEFs and nucleotide exchange/activation (Das et al., 2015). Rac1 is anchored to the inner leaflet of the plasma membrane through its prenylated C-terminus and polybasic motif (van Hennik et al., 2003), which permits interaction with the anionic phospholipids PIP2, PIP3 and phosphatidylserine (Finkielstein, Overduin, & Capelluto, 2006; Heo et al., 2006; Remorino et al., 2017). Localized clustering of PIP2, PIP3 and phosphatidylserine within the plasma membrane thus permits precise spatial and temporal distribution of Rac1 activation (Fairn et al., 2011; Kay,

Koivusalo, Ma, Wohland, & Grinstein, 2012; Remorino et al., 2017). Rac1 activation gradients within heterogeneous signaling nanodomains in turn regulate cytoskeletal rearrangement, lamellipodia formation and migration through binding to WASP-family verprolin-homologous (WAVE) proteins and activation of the actin-related protein 2/3 (Arp2/3) protein complex (Ehrlich, Hansen, & Nelson, 2002; Machacek et al., 2009; Remorino et al., 2017; Ridley, 2011). However, despite its pivotal role in migration, the cellular mechanisms regulating local Rac1 clustering at the plasma membrane are still incompletely understood.

Another set of proteins that play a key role in regulating cellular migration is ion channels (Schwab, Fabian, Hanley, & Stock, 2012). Changes in ion channel expression and/or activity in cancer cells regulate the plasma membrane potential ($V_m$) and intracellular signaling cascades as a result of altered ion flux (Brackenbury, 2016; Prevarskaya, Skryma, & Shuba, 2018). Motile cancer cells possess a more depolarized $V_m$ compared to terminally-differentiated non-cancer cells (Yang & Brackenbury, 2013). The $V_m$ is functionally instructive in regulating cell cycle progression (Sundelacruz, Levin, & Kaplan, 2009), proliferation (Blackiston, McLaughlin, & Levin, 2009; Zhou et al., 2015), differentiation (Sundelacruz, Levin, & Kaplan, 2008), cytoskeletal reorganization (Chifflet, Correa, Nin, Justet, & Hernandez, 2004; Chifflet, Hernandez, & Grasso, 2005; Chifflet, Hernandez, Grasso, & Cirillo, 2003; Nin, Hernandez, & Chifflet, 2009; Szaszi, Sirokmany, Di Ciano-Oliveira, Rotstein, & Kapus, 2005), tissue morphogenesis, regeneration and tumorigenesis (Beane, Morokuma, Adams, & Levin, 2011; Beane, Morokuma, Lemire, & Levin, 2013; Cervera, Alcaraz, & Mafe, 2016; Chernet, Adams, Lobikin, & Levin, 2016; Chernet & Levin, 2014; Lobikin, Chernet, Lobo, & Levin, 2012; Lobikin et al., 2015). $V_m$ depolarization controls mitogenic signaling by promoting redistribution of phosphatidylserine and PIP2 in the inner leaflet of the plasma membrane, enhancing nanoclustering and activation of the small GTPase K-Ras (Zhou et al., 2015). However, the mechanisms by which $V_m$ regulates other

behaviors, including morphological changes and migration, and the dependency of $V_m$ on altered activity of specific ion channels expressed on non-excitable cells, remain unclear.

An important class of ion channels in the context of cellular migration is the voltage-gated $Na^+$ channels (VGSCs). VGSCs contain a pore-forming $\alpha$ subunit ($Na_v1.1$-$Na_v1.9$), together with one or more smaller $\beta$ subunits ($\beta1$-$\beta4$) (Brackenbury & Isom, 2011; Catterall, Goldin, & Waxman, 2003). The canonical function of VGSCs is to regulate $V_m$ depolarization during the rising phase of action potentials in electrically-excitable cells (Hille, 1992). In addition, VGSCs not only regulate neuronal pathfinding and migration (Brackenbury et al., 2010; Brackenbury, Yuan, O'Malley, Parent, & Isom, 2013; Patel & Brackenbury, 2015), but also regulate the migration of non-excitable cells (J. A. Black & Waxman, 2013). For example, the $Na_v1.5$ subtype is upregulated in breast cancer cells where it plays a critical role in promoting cellular migration, invasion and metastasis (Besson et al., 2015; Brackenbury, 2012; Brackenbury, Chioni, Diss, & Djamgoz, 2007; Fraser et al., 2005; Martin, Ufodiama, Watt, Bland, & Brackenbury, 2015; Nelson, Yang, Dowle, Thomas, & Brackenbury, 2015; Nelson, Yang, Millican-Slater, & Brackenbury, 2015; Roger, Besson, & Le Guennec, 2003). In non-excitable cancer cells, $Na_v1.5$ carries a small persistent inward $Na^+$ current, which would be expected to depolarize the $V_m$ at steady state (Roger et al., 2003; Yang et al., 2012). $Na_v1.5$ activity promotes motility and invasive behavior through several mechanisms, including MAPK activation (Carrie D House et al., 2010; C. D. House et al., 2015), up-regulation of CD44 expression (Nelson, Yang, Millican-Slater, et al., 2015), and potentiation of $Na^+/H^+$ exchanger type 1 (NHE1) activity leading to cysteine cathepsin activation (Brisson et al., 2013; Brisson et al., 2011; Gillet et al., 2009). $Na_v1.5$ also promotes acquisition of an elongate mesenchymal-like phenotype, cortactin phosphorylation and cytoskeletal reorganization (Brisson et al., 2013; Nelson, Yang, Millican-Slater, et al., 2015). Taken together, these data point to an important role for both $Na_v1.5$ and $V_m$ in regulating

morphological changes and migration. An important question is, therefore, how migratory behavior is regulated by electrical changes and $Na^+$ flux at the plasma membrane.

Here, we investigated the role of $Na_v1.5$ in regulating $V_m$ in non-excitable breast cancer cells. We report that $Na_v1.5$ promotes steady state $V_m$ depolarization, which in turn leads to localized activation of Rac1 at the plasma membrane, promoting morphological changes and migration. This work uncovers a novel and unexpected voltage-dependent mechanism for Rac1 activation, which would fine tune cell migration in response to ionic and/or electric field changes in the local microenvironment.

## Materials and Methods

### *Chemicals*

Iberiotoxin, NS-1619, tetrodotoxin (TTX) and veratridine were purchased from Alomone Labs. Phenytoin was from Sigma. Ionomycin was from Cayman Chemical. EHT1864 was from Santa Cruz Biotechnology. Drugs were reconstituted as stock solutions according to manufacturer guidelines and diluted directly into culture medium and/or recording solutions at the indicated working concentrations.

### *Cell culture*

MDA-MB-231 human breast cancer cells were cultured at 37°C, 5 % $CO_2$ in Dulbecco's modified eagle medium (DMEM) supplemented with 5% fetal bovine serum (FBS) and 4 mM L-glutamine. MDA-MB-231 cells are a well-established cell line for examining the functional activity of $Na_v1.5$ in regulating cell behavior and they demonstrate robust endogenous expression of this channel (Brackenbury et al., 2007; Brisson et al., 2013; Brisson et al., 2011; Fraser et al., 2005; Nelson, Millican-Slater, Forrest, & Brackenbury, 2014; Roger et

al., 2003; Yang et al., 2012). Cells were confirmed to be mycoplasma-free by the 4',6-diamidino-2-phenylindole (DAPI) staining method (Uphoff, Gignac, & Drexler, 1992). Molecular identity was confirmed by short tandem repeat analysis (Masters et al., 2001).

***RNA interference***

A GFP-expressing MDA-MB-231 cell line lacking functional $Na_v1.5$ expression was produced previously by transduction of recombinant lentivirus for shRNA targeting $Na_v1.5$ (MISSION pLKO.1-puro shRNA transduction particles; Sigma) (Nelson, Yang, Millican-Slater, et al., 2015). $Na_v1.5$-shRNA cells and cells non-targeting shControl cells were maintained in G418 (4 µl/ml, Sigma), blasticidin (2 µl/ml, AppliChem) and puromycin (0.1 µl/ml, Sigma).

***Whole-cell patch clamp recording***

The whole-cell patch clamp technique was used to record membrane current and voltage from cells grown on glass coverslips for 48-72 h. Voltage- and current-clamp recordings were made using a Multiclamp 700B amplifier (Molecular Devices) at room temperature. Membrane currents and $V_m$ were digitized using a Digidata 1440A interface (Molecular Devices), low-pass filtered at 10 kHz and analyzed using pCLAMP 10.4 software (Molecular Devices). In voltage-clamp mode, signals were sampled at 50 kHz, and the series resistance was compensated by 40-60 %. Linear components of leak were subtracted using a P/6 protocol (Armstrong & Bezanilla, 1977). The standard extracellular physiological saline solution (PSS) contained the following components (in mM): 144 NaCl, 5.4 KCl, 1 $MgCl_2$, 2.5 $CaCl_2$, 5 HEPES and 5.6 glucose adjusted to pH 7.2 with NaOH. For the $Na^+$-free PSS, NaCl was replaced with 144 mM N-methyl-D-glucamine (NMDG) or choline chloride (ChoCl) adjusted to pH 7.2 with HCl. The standard intracellular (pipette) solution contained (in mM) 5 NaCl, 145 KCl, 2 $MgCl_2$, 1 $CaCl_2$, 10 HEPES and 11 EGTA adjusted to pH 7.4 with KOH. Free $Ca^{2+}$ concentration in the solution was calculated using MaxChelator software (Stanford

University). $Na^+$ current was activated by depolarizing from -120 mV (250 ms) to voltages in the range -80 to +30 mV in 5 mV increments (50 ms).

***Membrane potential recording***

The steady-state $V_m$ was recorded in I = 0 mode within 5 s of achieving the whole-cell configuration. To monitor the continuous $V_m$ in individual cells in response to pharmacological treatments, cells were held in the whole-cell configuration for 6 min, with 60 s in the standard PSS, followed by 150 s in treatment and a further 150 s for washout of treatment. Where relevant, a vehicle treatment control was included in each experiment. The mean $V_m$ over the last 5 s in each of the three stages was used to compare the $V_m$ data. The $V_m$ signals were sampled at 200 Hz. Liquid junction potentials were calculated using the integrated tool in Clampex 10.4. Dose-response data were fitted to a sigmoidal logistic equation

$$\%\, block = \frac{100}{1 + (\frac{IC_{50}}{[Drug]})^n}$$

where $IC_{50}$ is the concentration of drug at which half of its maximal effect occurs; and n is the slope giving the Hill coefficient.

***Perforated patch clamp recordings***

The perforated patch clamp technique was used to record $K_{Ca}1.1$ currents. The intracellular solution used in perforated patch recording contained (in mM) 5 choline-Cl, 145 KCl, 2 $MgCl_2$, 10 HEPES and 1 EGTA adjusted to pH 7.4 with KOH. Nystatin (150 μM) in DMSO was made up and added to the perforated patch intracellular solution on the day of the experiment. Typical series resistance ranged between 20-40 MΩ. $K_{Ca}1.1$ currents were elicited by depolarizing from -120 mV (250 ms) to voltages in the range -60 to +90 mV in 10

mV increments (300 ms). The outward current data were fitted to a single exponential decay (Sanguinetti & Jurkiewicz, 1990)

$$Y = Y_0 \times e^{kx}$$

where k is the rate constant.

### *Intracellular $Na^+$ and $Ca^{2+}$ imaging*

Measurement of $[Na^+]_i$ was performed as described in (Roger et al., 2007) with minor modifications. Briefly, 6 × $10^4$ cells grown on glass coverslips for 24 h were labelled with 5 μM SBFI-AM (Sigma) and 0.1 % v/v Pluronic F-127 (Life Technologies) in DMEM with 0 % FBS at 37 °C in the dark for 1 h. Excess SBFI-AM was washed out with 37 °C DMEM supplemented with 5 % FBS. The coverslip was assembled into a RC-20H closed bath imaging chamber (Warner Instruments) and observed at room temperature using a Nikon Eclipse TE200 epifluorescence microscope at 40X. SBFI was alternately excited at 340 and 380 nm, and the fluorescence emission at 510 nm was collected at 8-bit depth using a Rolera-XR Fast 1394 CCD camera (QImaging) controlled by SimplePCI software (Hamamatsu). Calibration of $[Na^+]_i$ was performed after each recording by perfusing two solutions on the cells: 10 and 20 mM $Na^+$. They contained (in mM) 149.4 NaCl + KCl, 1 $MgCl_2$, 2.5 $CaCl_2$, 5 HEPES, 5.6 glucose and 0.02 gramicidin (Sigma), adjusted to pH 7.2 with KOH. In each experimental repeat, $[Na^+]_i$ of ≥ 7 individual cells in the field of view were calculated individually and then averaged. For $Ca^{2+}$ imaging, cells were labelled with 1 μM Fura-2 AM (PromoKine) using the same procedure as above, with an additional wash step using 37 °C phenol red-free DMEM (Life Technologies) after 1 h incubation with the dye, and the images were captured at 20X. In each experimental repeat, the $[Ca^{2+}]_i$ of ≥ 17 individual cells in the field of view were measured. Each experiment was repeated at least three times.

### *Western blotting*

Western blotting was performed as described previously (Nelson et al., 2014). The primary antibodies were mouse anti-$K_{Ca}1.1$ (1:500; NeuroMab) and mouse anti-$\alpha$-tubulin (1:10,000; Sigma).

***Cell migration assay***

Cell migration was measured using wound healing assays (Yang et al., 2012). Label-free ptychographic microscopy was used to monitor motility in real time (Marrison, Raty, Marriott, & O'Toole, 2013; Suman et al., 2016). Images were acquired over 16 h at 9 min intervals using a Phasefocus VL-21 microscope with an 10X (0.25 NA) lens using 640 nm illumination and equipped with an environmental chamber maintaining the cells at 37 °C in 5% $CO_2$. The wound healing experiment was repeated three times on separate days. Image sequences of gap closure were processed using Phasefocus Cell Analysis Toolbox (CAT) software in order to segment and track individual cells at the leading edge and measure wound area. For each image sequence, the following parameters were automatically measured: change in normalized gap area over time; $t_{1/2}$ for gap closure (h), determined by applying a linear fit to the normalized wound area reduction from t = 0 until the time at which the area reduces by 50 %; collective migration (μm/h), defined as:

$$V_{migration} = \frac{|slope|}{2 \times l}$$

where slope is the rate of area of scratch closure and l is the length of the scratch; instantaneous velocity per cell (μm/s), considering segmented cells with track lengths of ≥ 5 frames; and directionality of leading-edge cells tracked for ≥ 5 frames, relative to the center of the scratch.

***Cell proliferation and invasion assays***

Cell proliferation was measured using the thiazolyl blue tetrazolium bromide (MTT) assay, as described (Yang et al., 2012). Cell invasion was quantified using 24-well Corning BioCoat Matrigel Invasion Chambers according to the manufacturer's guidelines. Briefly, $2.5 \times 10^4$ MDA-MB-231 cells were seeded in the upper compartment supplemented with 1 % FBS and appropriate treatments. The lower compartment contained 10 % FBS and appropriate treatments. Cells were incubated at 37 °C for 24 h before the removal of non-invaded cells from the upper chamber using cotton buds. Cells that had invaded through the polyethylene terephthalate membrane were fixed using 4 % paraformaldehyde for 10 min and were washed three times with phosphate buffered saline (PBS), 5 min/time, before staining with DAPI. The membrane was then mounted on a glass microscope slide. DAPI-positive cells on the membrane were viewed at 20X using a Nikon Eclipse TE200 epifluorescence microscope. Experiments were performed on duplicate wells and repeated ≥ 3 times.

***Immunocytochemistry***

Cells ($1.6 \times 10^5$) were cultured on glass coverslips in 4-well plates for 48 h in order to form confluent monolayers. Wounds were made on the coverslip using a P200 pipette tip and debris was washed off with 37 °C DMEM. Appropriate treatments were subsequently applied, and cells were allowed to migrate into the wound for 3 h. This incubation duration was used because it was long enough to show an effect of $V_m$ inhibition on migration. Cells were fixed in 4 % paraformaldehyde for 10 min and immunocytochemistry was performed, as described (Nelson et al., 2014). The following primary antibodies were used: rabbit anti-$Na_v1.5$ (1:100; Alomone); rabbit anti-$K_{Ca}1.1$ (1:100; Neuromab); mouse anti-Rac1-GTP (1:500; NewEast Biosciences); rabbit anti-total Rac1 (1:10; NewEast Biosciences); mouse anti-CD44 (1:100; AbD Serotec). The secondary antibodies were Alexa 488 or 568-conjugated goat anti-mouse and Alexa 488 or 568-conjugated goat anti-rabbit (1:500; Life Technologies). In some experiments, cells were counter-stained with Alexa 633-conjugated phalloidin (1:50; Life Technologies). In experiments where permeabilized cells were labelled

with Alexa 568-conjugated annexin V (1:20; Life Technologies), primary and secondary antibodies were incubated in $Ca^{2+}$-containing annexin V binding buffer (Life Technologies) to preserve annexin V binding. Coverslips were then mounted on glass microscope slides using Prolong Gold with DAPI (Life Technologies). The slides were examined using a Zeiss LSM 710 confocal microscope at 40X. Confocal images were acquired sequentially for each channel. Images (512 x 512 or 1024 x 1024 pixels, dependent on experiment) were initially processed with the Zeiss Zen 2 software, and later exported into ImageJ for analysis. Brightness/contrast was adjusted using the ImageJ "Auto" function.

***Morphology and lamellipodium scoring***

Circularity was calculated on manually segmented cells using the free-hand tool in ImageJ (Schneider, Rasband, & Eliceiri, 2012):

$$Circularity = 4\pi \times \frac{Area}{Perimeter^2}$$

Values approaching 0 indicate a more elongated cell morphology. Feret's diameter was measured as the maximum distance between any two points along the cell boundary. Three experimental repeats were performed, and 20-25 cells per condition were analyzed for every repeat. To score lamellipodia formation, cells were categorized into two groups: with and without lamellipodium. For each of the three experimental repeats, 40-50 cells per condition were analyzed blinded to treatment.

***Analysis of Rac1 localization in the lamellipodium***

The signal densities of F-actin, Rac1-GTP and total Rac1 in the lamellipodium were analyzed in arcs at various distances from the leading edge as described (Dang et al., 2013). The region of interest in the lamellipodia was determined by the dense staining of F-actin. To avoid bias in choosing ROIs, the analysis was carried out blinded to treatment. The

ImageJ Radial Profile Extended plugin (Philippe Carl, CNRS, France) was used with starting radius = 0.43 μm, radius increment = 0.43 μm, ending radius = 5.6 μm and total integrated angle = 90°, resulting in 13 arcs in total. Signal densities on each of the arcs were obtained and were normalized to those on the innermost arc. Typically, 20-30 cells at the edge of the wound were analyzed for each condition and the experiment was repeated three times.

***Colocalization analysis***

Colocalization of annexin V and Rac1-GTP labeling within regions of interest drawn around the lamellipodium was evaluated using the Coloc2 plugin in ImageJ. The approximate point spread function on acquired images of 1024 x 1024 pixels was 2.71 pixels. For each region of interest, the thresholded Manders M1 and M2 coefficients for annexin V and Rac1-GTP were computed (Manders, Verbeek, & Aten, 1993), together with the Li's intensity correlation coefficient (Li et al., 2004). Measurements were taken from 30 cells per condition over three experimental repeats.

***In vitro Rac1 activity assay***

Cells were cultured to 70 % confluency in 6-well plates prior to addition of pharmacological treatment(s). After incubation for 24 h, total cellular Rac1 activity was evaluated in cell lysates using a colorimetric ELISA-based small GTPase activation assay, according to the manufacturer's instructions (G-LISA; Cytoskeleton, Inc) (Antonov et al., 2012). Measurements were obtained from duplicate wells and the experiment was repeated three times.

***Live cell imaging of Rac1 biosensor activation***

Cells (1.6 x $10^5$) were cultured in 8-well chamber glass slides. After incubation for 24 h, cells were transfected with 200 ng of a biosensor for Rac1 activation (pTriEx4-Rac1-2G; Addgene plasmid # 66110) (Fritz et al., 2015) using Fugene (Roche) (Nelson et al., 2014). 48 h following transfection, appropriate treatments in phenol red-free DMEM were applied for 3 h prior to imaging. FRET imaging of biosensor activation was performed at room temperature using a Nikon Eclipse TE200 epifluorescence microscope with a 40X (NA 0.60) objective. Acquisition from cells expressing low levels of the biosensor was performed at 8-bit depth using a Rolera-XR Fast 1394 CCD camera (QImaging) controlled by SimplePCI software (Hamamatsu). Acquisition time for donor and FRET channels was typically 200 ms. The donor and acceptor channels were acquired sequentially. The donor, monomeric teal fluorescent protein (mTFP), was excited at 436 nm and emission was collected at 480 nm. FRET emission was collected above 540 nm. The acceptor (Venus) was excited at 480 nm and emission collected above 540 nm. Visualization of cells transfected with a control plasmid expressing mTFP alone, created by site-directed mutagenesis (Nelson et al., 2014), revealed minimal bleed-through in the FRET and Venus channels. Images were taken from ≥49 cells across three experimental repeats. Image processing was performed using ImageJ. Cells were manually segmented using the distribution of biosensor (donor mTFP signal). Images were then background subtracted prior to calculation of the FRET/mTFP integrated density ratio for each cell.

***Statistics***

Data are presented as mean ± SEM. GraphPad Prism 7.0d was used to perform all statistical analyses. Polar histograms were plotted using OriginLab Origin 2017. For normally distributed data, paired or unpaired Student's two-tailed t-test was used to compare two groups, as appropriate. Multiple comparisons were made using 1-way ANOVA or repeated measures ANOVA followed by Tukey *post-hoc* tests, as appropriate. For repeated measures data that were not normally distributed, a Friedman test with Dunn's *post-hoc* tests was

used. Fisher's exact test was used to examine the distribution of samples within a population. Contingency table data were analyzed using $\chi^2$ test. Colocalization data were analyzed by 2-way ANOVA. Results were considered significant at $P < 0.05$.

## Results

### *$Na_v1.5$ channels depolarize the membrane potential of breast carcinoma cells*

The $V_m$ of motile cancer cells is generally more depolarized than in terminally-differentiated non-cancer cells (Yang & Brackenbury, 2013). In addition, both depolarized $V_m$ and $Na_v1.5$ channel activity correlate with metastatic potential (Fraser et al., 2005). However, it is not known whether the relationship between $Na_v1.5$, $V_m$ and cell behavior is causal. Here, we first investigated whether $Na^+$ conductance through plasma membrane $Na_v1.5$ channels contributes to the depolarized $V_m$ that has been reported previously in MDA-MB-231 cells (Fraser et al., 2005). $Na_v1.5$ carries a persistent inward $Na^+$ current, small in amplitude compared to the transient $Na^+$ current, which plays an important role in shaping the action potential firing pattern, especially in the subthreshold voltage range (George, 2005). In non-excitable cells, this would allow significant accumulation of $Na^+$ over an extended period, potentially permitting $V_m$ depolarization at steady state. $Na_v1.5$ is robustly expressed in MDA-MB-231 cells, both in intracellular compartments and at the plasma membrane (Figure 1A). This agrees with previous reports of VGSC distribution in non-excitable cells (Brisson et al., 2013; Brisson et al., 2011; Carrithers et al., 2009; Carrithers et al., 2007; Fraser et al., 2005; Nelson, Yang, Millican-Slater, et al., 2015; Persson et al., 2014; Yang et al., 2012). We measured $Na^+$ currents carried by $Na_v1.5$ using whole-cell voltage clamp recording. Depolarization from -120 mV to -10 mV elicited both transient and persistent inward $Na^+$ currents (Figure 1B, C). Analysis of the voltage-dependent activation and steady-state inactivation of the $Na^+$ current revealed a window current between -50 mV and -10 mV

(Figure 1D, E). We next investigated whether $Na_v1.5$ could regulate the $V_m$. Stable suppression of $Na_v1.5$ expression using lentiviral shRNA (Nelson, Yang, Millican-Slater, et al., 2015) significantly hyperpolarized the $V_m$ compared to control cells, measured using whole-cell current clamp recording, from -12.6 ± 0.9 mV to -16.0 ± 0.8 mV ($P < 0.01$; n = 16; t test; Figure 1F). Thus, $Na_v1.5$ is required to depolarize the steady-state $V_m$.

We next evaluated the effect of pharmacologically perturbing $Na_v1.5$ activity. The specific VGSC blocker TTX (30 μM) reversibly inhibited the transient and persistent $Na^+$ current ($P < 0.001$ and $P < 0.05$, respectively; n ≥ 5; repeated measures ANOVA with Tukey test; Figure 2A-D), consistent with previous reports (Brackenbury et al., 2007; Fraser et al., 2005; Roger et al., 2003). TTX also significantly hyperpolarized the $V_m$ from -13.2 ± 1.3 mV to -17.5 ± 1.6 mV ($P < 0.01$; n = 17; repeated measures ANOVA with Tukey test; Figure 2E, F). On the other hand, the carrier for TTX (148 μM sodium citrate, pH = 4.8) had no effect on the $V_m$ (Figure S1A, B). In agreement with the TTX data, the VGSC-inhibiting antiepileptic drug, phenytoin (100 μM) also significantly reduced the transient and persistent $Na^+$ current and hyperpolarized the $V_m$ (Figure S1C-K). In contrast, veratridine (100 μM), which increases channel open probability by inhibiting inactivation (Ulbricht, 1998), increased the persistent $Na^+$ current (Figure 2G, H and Figure S2A, B) and depolarized the $V_m$ from -16.37 ± 1.4 mV to -12.6 ± 1.3 mV ($P < 0.05$; n = 13; t test; Figure 2H). In summary, these data show that pharmacological or genetic inhibition of $Na_v1.5$ hyperpolarizes the steady-state $V_m$, whereas increasing the persistent $Na^+$ current depolarizes the $V_m$. Thus, persistent current carried by $Na_v1.5$ contributes to $V_m$ depolarization.

***Membrane potential depolarization is dependent on extracellular $Na^+$***

To evaluate the sufficiency of extracellular $Na^+$ to determine the $V_m$, we next removed $Na^+$ in the extracellular solution during recording. Replacement of extracellular NaCl with choline chloride reversibly hyperpolarized the $V_m$ from -10.4 ± 1.0 to -20.4 ± 2.0 mV ($P < 0.001$; n =

10; repeated measures ANOVA with Tukey test; Figure 3A, B). Using NMDG to replace extracellular $Na^+$ had a similar hyperpolarizing effect (Figure S2C, D). Thus, extracellular $Na^+$ is required for steady-state $V_m$ depolarization.

Inward $Na^+$ current through $Na_v1.5$ channels would be expected to elevate the intracellular $Na^+$ level ($[Na^+]_i$]) at steady state. Indeed, VGSCs have previously been shown to increase $[Na^+]_i$ (Campbell, Main, & Fitzgerald, 2013; Roger et al., 2007). We therefore next investigated the involvement of extracellular $Na^+$ in setting $[Na^+]_i$ using the ratiometric $Na^+$ indicator SBFI-AM (Figure 3C, D). Replacement of extracellular $Na^+$ with NMDG significantly reduced the steady-state $[Na^+]_i$ from 15.6 ± 1.7 mM to 7.6 ± 2.9 mM ($P < 0.001$; $n = 3$; ANOVA with Tukey test; Figure 3E). Treatment with TTX also significantly reduced the steady-state $[Na^+]_i$, suggesting that $Na_v1.5$ activity contributes to this elevation of $[Na^+]_i$ ($P < 0.05$; $n \geq 10$; ANOVA with Tukey test; Figure 3E). In agreement with this, the $[Na^+]_i$ of $Na_v1.5$-shRNA cells was significantly lower than for control cells (9.4 ± 1.2 mM *vs.*13.5 ± 0.6 mM; $P < 0.01$; $n = 3$; t test; Figure 3F). On the other hand, $Na_v1.5$ inhibition with TTX had no effect on $[Ca^{2+}]_i$ (Figure S3A-D). Together, these data suggest that $Na^+$ influx through $Na_v1.5$ channels increases $[Na^+]_i$, but not $[Ca^{2+}]_i$.

***$K_{Ca}$1.1 regulates the membrane potential but not the $Na^+$ level***

$Na_v1.5$ channels enhance cell migration, invasion, tumor growth and metastasis (Fraser et al., 2005; Nelson, Yang, Millican-Slater, et al., 2015; Roger et al., 2003). Given that $Na_v1.5$ depolarizes the steady-state $V_m$, and that $V_m$ depolarization is functionally instructive in regulating cellular behavior (Yang & Brackenbury, 2013), we reasoned that $Na_v1.5$ may regulate cell migration via setting the $V_m$. Thus, we sought a means by which to manipulate the $V_m$ independent of $Na_v1.5$ in order to separate the effects of $V_m$ and $[Na^+]_i$ on downstream signaling. To do this, we took advantage of ubiquitously expressed large conductance $Ca^{2+}$-activated $K^+$ channel, $K_{Ca}1.1$ (Contreras et al., 2013). We verified that

$K_{Ca}1.1$ was robustly expressed in MDA-MB-231 cells (Khaitan et al., 2009; Ma et al., 2012; Roger, Potier, Vandier, Le Guennec, & Besson, 2004), and its expression was unaffected by $Na_v1.5$ downregulation (Figure 4A, B). Next, using the perforated patch clamp mode to maintain endogenous $[Ca^{2+}]_i$, we found that the $K_{Ca}1.1$ opener NS-1619 (1 μM) (Macmillan, Sheridan, Chilvers, & Patmore, 1995) increased outward $K^+$ current, confirming $K_{Ca}1.1$ activity (Figure 4C, D). Co-application of the $K_{Ca}1.1$ channel blocker iberiotoxin (100 nM) inhibited the potentiating effect of NS-1619 on the outward current (Figure 4C, D), confirming specificity of NS-1619. We next studied the effect of NS-1619 on the $V_m$. NS-1619 hyperpolarized the steady-state $V_m$ in a dose-dependent manner (Figure 4E). Importantly, 1 μM NS-1619 hyperpolarized the $V_m$ by 4.4 mV from -10.6 ± 1.3 mV to -15.0 ± 0.6 mV ($P < 0.01$; $n \geq 12$; t test; Figure 4F). This shift is equivalent to the hyperpolarization elicited by inhibiting $Na_v1.5$ activity (Figure 2F, I). In contrast, NS-1619 treatment did not significantly alter the $[Na^+]_i$ ($P = 0.93$; $n = 22$; paired t test; Figure 4G) or $[Ca^{2+}]_i$ (Figure S3E, F). Finally, the $V_m$ recorded using the standard intracellular solution (free $[Ca^{2+}] = 5.7$ nM) was not significantly different from that recorded using intracellular solution with 100 nM free $[Ca^{2+}]$ ($P = 0.82$; $n = 12$; t-test; Figure 4H), suggesting that at physiological $[Ca^{2+}]_i$ (Sareen, Darjatmoko, Albert, & Polans, 2007; Winnicka, Bielawski, Bielawska, & Surazynski, 2008), $K_{Ca}1.1$ channels do not contribute to regulating the $V_m$ in the absence of NS-1619. In summary, activation of $K_{Ca}1.1$ hyperpolarizes the $V_m$ to the same extent as $Na_v1.5$ inhibition, thus providing an experimental means by which to manipulate the $V_m$ independent of $Na^+$.

***$Na_v1.5$-dependent membrane potential depolarization regulates cell migration and morphology***

Using NS-1619 and TTX as tools to modify the $V_m$ independent of, or as a result of $Na_v1.5$ activity, respectively, we next investigated the effect of $V_m$ depolarization on cell migration in wound healing assays using label-free ptychographic imaging (Figure 5A). Both TTX and NS-1619 slowed the rate of wound closure (Figure 5B). The $t_{1/2}$ of wound closure increased

from 5.7 ± 1.1 h to 9.8 ± 0.7 h in the presence of TTX and 9.9 ± 0.1 h in the presence of NS-1619 ($P < 0.05$; $n \geq 5$; ANOVA with Tukey test; Figure 5C). Similarly, the collective migration of cells moving into the wound was reduced from 7.8 ± 0.7 μm/h to 5.5 ± 0.4 μm/h in the presence of TTX and 4.9 ± 0.5 μm/h in the presence of NS-1619 ($P < 0.05$; $n \geq 5$; ANOVA with Tukey test; Figure 5D). The instantaneous velocity of individual cells at the leading edge was also reduced from $6.2 \times 10^{-3} \pm 5.6 \times 10^{-5}$ μm/s to $4.7 \times 10^{-3} \pm 5.0 \times 10^{-5}$ μm/s and $4.4 \times 10^{-3} \pm 4.5 \times 10^{-5}$ μm/s, for TTX- and NS-1619-treated cells, respectively ($P < 0.001$; $n \geq 2662$; Kruskal-Wallis with Dunn's test; Figure 5E). In addition, both TTX and NS-1619 caused a small, but statistically significant, disruption in the directionality of cells at the leading edge, reducing the proportion of cells migrating directly into the wound ($P < 0.001$; Friedman with Dunn's test; Figure 5F). Hyperpolarizing the $V_m$ with NS-1619 did not significantly alter cell proliferation measured in an MTT assay (Figure S4A). Given that inhibiting $Na_v1.5$ with TTX has no effect on the proliferation of MDA-MB-231 cells (Fraser et al., 2005; Gillet et al., 2009; Roger et al., 2003), together, these data suggest that both $Na_v1.5$ activity and $V_m$ depolarization promote cellular migration, without affecting proliferation. On the other hand, whilst TTX significantly reduced invasion into Matrigel, consistent with previous reports (Brackenbury et al., 2007; Driffort et al., 2014; Fraser et al., 2005; Nelson, Yang, Millican-Slater, et al., 2015; Roger et al., 2003; Yang et al., 2012), NS-1619 had no effect (Figure S4B, C). Thus, $Na_v1.5$ promotes cellular migration via $V_m$ depolarization, whereas $Na_v1.5$-dependent promotion of invasion occurs via a $V_m$-independent mechanism.

$Na_v1.5$ promotes an elongate, mesenchymal-like motile morphology (Brisson et al., 2013; Driffort et al., 2014; Nelson, Yang, Millican-Slater, et al., 2015). This morphological modulation has been shown to occur through two potentially overlapping mechanisms: (1) regulation of adhesion-mediated signaling *via* β1 subunits and up-regulation of CD44 expression (Nelson et al., 2014; Nelson, Yang, Millican-Slater, et al., 2015), and (2) *via* increased Src kinase activity, phosphorylation of the actin-nucleation-promoting factor

cortactin, and F-actin polymerization (Brisson et al., 2013). In addition, the $V_m$ has been shown to promote reorganization of the actin filament network and cytoskeleton in other cell types (Chifflet et al., 2004; Chifflet et al., 2005; Chifflet et al., 2003; Nin et al., 2009; Szaszi et al., 2005). However, the potential involvement of $V_m$ in $Na_v1.5$-mediated signaling is not known. We thus investigated the participation of $Na_v1.5$-mediated $V_m$ depolarization in regulating cell morphology. TTX (30 μM) significantly increased cell circularity after 3 h ($P < 0.001$; $n \geq 61$; ANOVA with Tukey test; Figure 6A, B), consistent with previously published data (Brisson et al., 2013). NS-1619 (1 μM) also increased circularity ($P < 0.05$; $n \geq 61$; ANOVA with Tukey test; Figure 6A, B). Similarly, TTX and NS-1619 both significantly reduced the Feret's diameter (maximum caliper distance across the cell; $P < 0.01$; $n \geq 57$; ANOVA with Tukey test; Figure 6C). These data suggest that $V_m$ depolarization promotes acquisition of an elongate phenotype.

Given that $Na_v1.5$-mediated $V_m$ depolarization promotes both morphological changes and cellular migration, we postulated that it might regulate formation of lamellipodia in migrating cells. We therefore scored the number of migrating cells with visible lamellipodia in a wound healing assay following treatment with TTX and NS-1619. Both treatments significantly reduced the proportion of cells with a lamellipodium in the measured population ($P < 0.001$; $n \geq 139$ cells per condition; $\chi^2$ test; Figure 6D). Together, these findings suggest that $Na_v1.5$-mediated $V_m$ depolarization promotes a change in cellular morphology towards an elongate phenotype, and increases lamellipodia formation, thus potentiating cellular migration.

***$Na_v1.5$-dependent membrane potential depolarization regulates Rac1 activation***

The small GTPase Rac1, together with Rho and cdc42, plays a critical role in regulating cytoskeletal organization and cell motility (Burridge & Wennerberg, 2004). In addition, Rac1 also regulates the formation of lamellipodia, cell motility and the directionality of cell

movement (Wu et al., 2009). We therefore postulated that $Na_v1.5$ and $V_m$ depolarization may regulate the level of active (GTP-bound) Rac1 in the lamellipodia of migrating cells. We treated migrating cells with NS-1619 and TTX for 3 h and then evaluated distribution of Rac1-GTP by quantifying immunocytochemical signal density across concentric arcs in the lamellipodium of individual cells (Figure 7A, B). As reported previously, a large quantity of Rac1 is present intracellularly in the perinuclear region, although there is also an enrichment of Rac1-GTP in the lamellipodium, consistent with its critical role in this region (Garcia-Mata et al., 2011; Wu et al., 2009). Both TTX and NS-1619 significantly reduced the peak Rac1-GTP signal at the leading edge of migrating cells ($P < 0.05$; $n \geq 66$; 1-way ANOVA with Tukey test; Figure 7C). However, the level of total cellular Rac1-GTP, determined in whole cell lysates, was unaffected by TTX treatment ($P = 0.80$; $n = 6$; t test; Figure 7D). Given that the majority of Rac1 is present intracellularly (Figure 7A) (Das et al., 2015; Moissoglu, Slepchenko, Meller, Horwitz, & Schwartz, 2006), these data suggest that $Na_v1.5$ may regulate Rac1 locally at the plasma membrane and/or within lamellipodia. We next evaluated the effect of TTX and NS-1619 on distribution of Rac1-GTP *vs.* total Rac1 using an antibody that does not distinguish between GDP- and GTP-bound forms of Rac1 (Figure 7E). The peak total Rac1 signal at the leading edge of migrating cells was unaffected by both TTX and NS-1619 ($P = 0.69$; $n \geq 60$; 1-way ANOVA; Figure 7F, G). Thus, the ratio of peak Rac1-GTP to total Rac1 at the leading edge was significantly reduced by both TTX and NS-1619 ($P < 0.001$; $n = 3$; 1-way ANOVA; Figure 7H). These data suggest that $V_m$ depolarization caused by steady state $Na_v1.5$ activity increases Rac1 activation at the leading edge of migrating cells.

$V_m$ depolarization promotes clustering and activation of the small GTPase K-Ras as a result of voltage-dependent redistribution of charged phospholipids including phosphatidylserine (Zhou et al., 2015). Given that Rac1 is also anchored to the inner leaflet of the plasma membrane via interaction with phosphatidylserine (Finkielstein et al., 2006; Magalhaes & Glogauer, 2010), we reasoned that a similar voltage-dependent mechanism may be

responsible for Rac1 activation in the lamellipodia. We therefore next evaluated the effect of $V_m$ depolarization on colocalization of Rac1-GTP with phosphatidylserine, using annexin V as a marker (Figure 8A). Treatment of migrating cells with TTX and NS-1619 reduced colocalization of Rac1-GTP with phosphatidylserine in the lamellipodia (Figure 8B-D). This was confirmed by quantification of thresholded Manders colocalization coefficients for phosphatidylserine and Rac1-GTP ($P < 0.01$; $n = 30$; 2-way ANOVA with Tukey test; Figure 8E). Similarly, the TTX and NS-1619 treatments both reduced the Li's intensity correlation quotient ($P < 0.001$; $n = 30$; 1-way ANOVA with Tukey test; Figure 8F). These data support the notion that $V_m$ depolarization increases Rac1 localization in the lamellipodia as a result of its interaction with phosphatidylserine.

In order to evaluate whether $Na_v1.5$-mediated $V_m$ depolarization promotes Rac1 activity in live cells, and to independently confirm the immunocytochemistry data, we next employed a genetically encoded Rac1 FRET biosensor to monitor Rac1 activation. In agreement with a previous report (Fritz et al., 2015), the biosensor showed a general gradient of Rac1 activation increasing from the cell interior towards the periphery, consistent with its critical role in actin remodeling at the edge of migrating cells (Figure 9A) (Wu et al., 2009). Treatment with TTX did not affect biosensor distribution (Figure 9A), but suppressed activation at the periphery (Figure 9B, C). Quantification of FRET across the whole cell revealed that TTX significantly reduced Rac1 activation to 48.6 ± 5.2 % of control ($P < 0.001$; $n \geq 49$; t test; Figure 9D). Together, these results indicate that blockade of $Na_v1.5$ channels suppresses Rac1 activation at the cell periphery.

***$Na_v1.5$-mediated morphological changes are dependent on Rac1 activation***

Given that $Na_v1.5$-dependent $V_m$ depolarization promotes morphological changes leading to increased cell migration (Figures 5, 6), and that $Na_v1.5$ promotes activation of Rac1 (Figures 7, 8, 9), which in turn, plays a key role in regulating cellular morphology and migration (Wu

et al., 2009), we analyzed the impact of Rac1 inhibition on $Na_v1.5$-dependent changes in cell morphology (Figure 10A). The specific Rac1 inhibitor EHT1864 increased circularity and reduced Feret's diameter in a dose-dependent manner (Figure S5A, B). Furthermore, EHT1864 increased circularity to a similar extent to TTX ($P < 0.001$; $n \geq 308$; 1-way ANOVA with Tukey test; Figure 10B, C). Importantly, co-application of EHT1864 with TTX had no additive effect on circularity or Feret's diameter (Figure 10B, C). These results show that Rac1 activity is required to transduce the $Na_v1.5$-dependent $V_m$ depolarizing signal in order to promote acquisition of an elongate, motile cell phenotype (Figure 10D).

## Discussion

Here we identify $Na_v1.5$-mediated $V_m$ depolarization as a regulator of Rac1 activation. Thus, we link ionic and electrical signaling at the plasma membrane to small GTPase-dependent cytoskeletal reorganization and cellular migration. We show that depletion of extracellular $Na^+$ or blockage of $Na_v1.5$ channels reversibly hyperpolarizes the $V_m$ at the timescale of minutes. We further show that $Na_v1.5$-dependent $V_m$ depolarization increases Rac1 colocalization with phosphatidylserine at the leading edge of migrating cells, promoting Rac1 activation, and resulting in acquisition of a motile, mesenchymal-like cellular phenotype. We therefore propose that $Na_v1.5$ may serve as a sensor for local changes in the ionic microenvironment, thus permitting voltage-dependent activation of Rac1 to fine tune cell migration.

### *Ion conductance, membrane potential and migration*

We show that $Na_v1.5$ carries a persistent inward $Na^+$ current in MDA-MB-231 cells. In agreement with the work of others, we report incomplete inactivation of $Na_v1.5$ resulting in a small voltage window encompassing the $V_m$, thus supporting this persistent $Na^+$ current (Brisson et al., 2011; Djamgoz & Onkal, 2013; Gillet et al., 2009; Nelson, Yang, Millican-

Slater, et al., 2015; Roger et al., 2003; Yang et al., 2012). The persistent inward $Na^+$ current carried by $Na_v1.5$ contributes to steady-state $V_m$ depolarization. Our findings agree with another study in H460 non-small cell lung cancer cells, in which $Na_v1.7$ channels were shown to depolarize the $V_m$ by ~10 mV (Campbell et al., 2013). Thus, the mechanism identified here is likely applicable to other non-excitable cell types where VGSCs are expressed (Chen et al., 2019; Grimes et al., 1995; Carrie D House et al., 2010; Persson et al., 2014; Zhou et al., 2015). In addition, it has previously been shown that VGSCs contribute to steady-state $V_m$ depolarization and viability in rat optic nerve axons and spinal cord astrocytes over a time course of hours (Sontheimer, Fernandez-Marques, Ullrich, Pappas, & Waxman, 1994; Stys, Sontheimer, Ransom, & Waxman, 1993), suggesting that this mechanism persists over an extended period. There may be other $Na^+$-permeable pathway(s) also contributing to $V_m$ regulation in non-excitable cells, e.g. via epithelial $Na^+$ channels (Amara, Ivy, Myles, & Tiriveedhi, 2015), $Na^+$-$K^+$ ATPase (Winnicka et al., 2008), and NHE1 (Brisson et al., 2011). The $V_m$ may also be dependent on the activity of transporters and channels regulating the movement of other ions, including $Cl^-$ and $K^+$ (Yang & Brackenbury, 2013). The depolarized resting $V_m$ reported here may therefore be attributed not only to the high permeability to $Na^+$ but also to the low expression/activity of hyperpolarizing $K^+$ channels.

Relatively small alterations in $V_m$ can be functionally significant. For example, during synaptic transfer from photoreceptors to ganglion cells in turtle retina, $V_m$ depolarizations as small as 5 mV are sufficient to activate paired ganglion cells (Baylor & Fettiplace, 1977). The $V_m$ can function as an instructive signal to regulate cell cycle progression in proliferating cells (Cervera et al., 2016; Cone, 1971; Cone & Cone, 1976; Zhou et al., 2015). $V_m$ depolarization can regulate other cellular behaviors, including differentiation (Sundelacruz et al., 2008) and cytoskeletal reorganization (Chifflet et al., 2004; Chifflet et al., 2005; Chifflet et al., 2003; Nin et al., 2009; Szaszi et al., 2005). At the tissue level, changes in $V_m$ can also regulate morphogenesis, regeneration and tumorigenesis (Beane et al., 2011; Beane et al., 2013;

Cervera et al., 2016; Chernet et al., 2016; Chernet & Levin, 2014; Lobikin et al., 2012; Lobikin et al., 2015). Several studies have shown that epithelial cells undergo $V_m$ depolarization when migrating into wounds (Chifflet et al., 2004; Chifflet et al., 2005). However, an interesting and novel finding of our study here is that $V_m$ depolarization is not simply a consequence of motile behavior (Schwab et al., 2012), but is *itself* a master regulator of morphological changes and migration. Here, we found that hyperpolarizing the $V_m$ by ~5 mV reduced migration by ~30 %. The fact that this level of $V_m$ hyperpolarization did not completely inhibit migration raises the possibility that additional hyperpolarization may have a further inhibitory effect. It is also likely that other ion conductance routes contributing to, and/or dependent on the $V_m$, may be involved in migration regulation. For example, hyperpolarization would increase the driving force for $Ca^{2+}$ entry. Nonetheless, our data underscore that persistent $Na^+$ influx through $Na_v1.5$ channels leads to $V_m$ depolarization, which in turn promotes cell migration.

Given the general trend towards depolarized $V_m$ both in cancer cells (Cervera et al., 2016; Fraser et al., 2005; Yang & Brackenbury, 2013), and in epithelial cells undergoing migration (Chifflet et al., 2004; Chifflet et al., 2005), we propose that voltage-dependent migratory behavior may be a general cellular phenomenon. For example, although involvement of $V_m$ was not directly investigated, activation of the $V_m$-hyperpolarizing channel $K_{Ca}1.1$ with NS-1619 reduces migration of glioma cells (Kraft et al., 2003). Furthermore, VGSCs have been detected in cells from a broad range of tumor types, where they potentiate migration and invasion (Besson et al., 2015; Brackenbury, 2012). We therefore argue that the results presented here have broad applicability to other cell types.

***Voltage-dependent regulation of Rac1 activation***

$V_m$ depolarization promotes K-Ras clustering and subsequent activation (Zhou et al., 2015). Various small GTPases, including K-Ras and the Rho GTPases, are anchored to the inner

leaflet of the plasma membrane through interaction with the anionic phospholipids PIP2, PIP3 and phosphatidylserine (Finkielstein et al., 2006; Heo et al., 2006; Magalhaes & Glogauer, 2010; Remorino et al., 2017; Zhou et al., 2015). In the case of K-Ras, clustering and activation has been shown using electron microscopy to arise as a result of depolarization-induced nanoscale redistribution of phosphatidylserine and PIP2 in the inner leaflet of the phospholipid bilayer, to which the K-Ras is anchored (Zhou et al., 2015). Our major discovery here is that Rac1 activation is also voltage-dependent. Our data show that $Na_v1.5$-mediated $V_m$ depolarization causes Rac1 activation, likely as a result of voltage-dependent redistribution of phosphatidylserine (Figure 10D). Thus, $V_m$-dependent signaling is not exclusively limited to mitogenic cascades but is also a key regulator of morphological changes and migration.

A growing body of evidence implicates $V_m$ depolarization in regulation of small GTPase activity. For example, $V_m$ has been shown to regulate the activity of GEF-H1, which, in turn, regulates the activity of the Rho/Rho kinase pathway (Waheed et al., 2010). $V_m$ depolarization-dependent activation of Rho and subsequent cytoskeletal organization has been shown to be $Ca^{2+}$-independent (Szaszi et al., 2005). In agreement with this, our data also imply that $Ca^{2+}$ is not involved as a signaling intermediary in $V_m$ depolarization-induced Rac1-mediated promotion of migration. On the other hand, in ATP-stimulated microglia, VGSC activity increases $[Ca^{2+}]_i$, and activates ERK and Rac1, promoting migration (Persson et al., 2014). $V_m$ depolarization-induced activation of Ras and Rap1 has also been reported in mouse cortical neurons (Baldassa, Zippel, & Sturani, 2003).

The mechanism uncovered here may feed into, and interact with, additional signaling pathways which have been shown to be dependent on $Na_v1.5$ activity. For example, $Na_v1.5$ has been shown to promote Src kinase activity and phosphorylation of cortactin and cofilin (Brisson et al., 2013). Thus, $Na_v1.5$-induced $V_m$ depolarization may activate Rac1, increasing cortactin phosphorylation and therefore enhancing cofilin activity and actin filament

polymerization. Src has also been shown to regulate Rac1 activity, suggesting the potential for feedback regulation (Servitja, Marinissen, Sodhi, Bustelo, & Gutkind, 2003). $Na_v1.5$ positively regulates the expression of the metastasis-promoting protein CD44, which may activate Src and therefore contribute to this process (Bourguignon, Zhu, Shao, & Chen, 2001; Carrie D House et al., 2010; C. D. House et al., 2015; Lee, Wang, Sudhir, & Chen, 2008; Nelson, Yang, Millican-Slater, et al., 2015). In addition, $Na_v1.5$ is expressed on astrocytes where it regulates migration by promoting reverse $Na^+/Ca^{2+}$ exchange (J. A. Black, Dib-Hajj, Cohen, Hinson, & Waxman, 1998; Pappalardo, Samad, Black, & Waxman, 2014). Furthermore, $Na_v1.5$ is expressed on the endosome of macrophages, where it regulates endosomal acidification (Carrithers et al., 2007). On the other hand, $Na_v1.6$ is expressed within macrophage podosomes, where it promotes invasion via intracellular $Na^+$ release (Carrithers et al., 2009). $Na_v1.5$ and $Na_v1.6$ are also expressed on microglia, where the latter has been shown to also regulate migration and cytokine release (Joel A. Black, Liu, & Waxman, 2009). It remains unknown whether $Na_v1.5$ opening changes during migration and what the signals might be that would regulate such alterations; however, it has been shown that $Na_v1.5$ can be regulated by growth factors and hormone signaling, and is itself mechanosensitive (Beyder et al., 2010; Fraser et al., 2014). Together, these studies suggest that VGSCs may further regulate the behavior of non-excitable cells via pathways in addition to the one identified here.

***Implications for our understanding of metastasis***

We provide evidence that $Na_v1.5$ contributes to steady-state $V_m$ depolarization, which in turn promotes $V_m$-dependent Rac1 activation, lamellipodial protrusion formation and cellular migration. These data are in agreement with the previously reported role for VGSCs in regulating morphology and migration of tumor cells (Brackenbury et al., 2007; Brackenbury & Djamgoz, 2006; Brisson et al., 2013; Fraser, Ding, Liu, Foster, & Djamgoz, 1999; Fraser et al., 2005; Nelson, Yang, Dowle, et al., 2015). It is therefore conceivable that depolarization-

dependent Rac1 activation may contribute to metastatic dissemination in response to local ionic changes in the tumor microenvironment. Thus, pharmacological targeting of VGSCs, which inhibits metastasis in preclinical models (Driffort et al., 2014; Nelson, Yang, Dowle, et al., 2015; Yildirim, Altun, Gumushan, Patel, & Djamgoz, 2012), may provide therapeutic benefit via $V_m$ hyperpolarization and downregulation of $V_m$-dependent small GTPase activation. In conclusion, our results reveal a new role for $Na_v1.5$ channels as voltage-dependent activators of Rac1 signaling to promote cellular migration.

**Disclosure Statement**

The authors have no conflicts of interest to declare.

**Author contributions**

MY and WB contributed to the conception and design of the work. MY, AJ, RK, RS, PO'T and WB contributed to acquisition, analysis, and interpretation of data for the work. MY, RK, RS, PO'T and WB contributed to drafting the work and revising it critically for important intellectual content. All authors approved the final version of the manuscript.

**References**


Amara, S., Ivy, M. T., Myles, E. L., & Tiriveedhi, V. (2015). Sodium channel gammaENaC mediates IL-17 synergized high salt induced inflammatory stress in breast cancer cells. *Cellular Immunology*. doi:10.1016/j.cellimm.2015.12.007

Antonov, A. S., Antonova, G. N., Fujii, M., ten Dijke, P., Handa, V., Catravas, J. D., & Verin, A. D. (2012). Regulation of endothelial barrier function by TGF-beta type I receptor ALK5: potential role of contractile mechanisms and heat shock protein 90. *Journal of Cellular Physiology, 227*(2), 759-771. doi:10.1002/jcp.22785

Armstrong, C. M., & Bezanilla, F. (1977). Inactivation of the sodium channel. II. Gating current experiments. *Journal of General Physiology, 70*(5), 567-590. Retrieved from http://www.ncbi.nlm.nih.gov/entrez/query.fcgi?cmd=Retrieve&db=PubMed&dopt=Citation&list_uids=591912

Baldassa, S., Zippel, R., & Sturani, E. (2003). Depolarization-induced signaling to Ras, Rap1 and MAPKs in cortical neurons. *Brain Research: Molecular Brain Research, 119*(1), 111-122. Retrieved from http://www.ncbi.nlm.nih.gov/pubmed/14597235

Baylor, D. A., & Fettiplace, R. (1977). Transmission from photoreceptors to ganglion cells in turtle retina. *Journal of Physiology, 271*(2), 391-424. Retrieved from http://www.ncbi.nlm.nih.gov/pubmed/200736

Beane, W. S., Morokuma, J., Adams, D. S., & Levin, M. (2011). A chemical genetics approach reveals H,K-ATPase-mediated membrane voltage is required for planarian head regeneration. *Chemistry & Biology, 18*(1), 77-89. doi:10.1016/j.chembiol.2010.11.012

Beane, W. S., Morokuma, J., Lemire, J. M., & Levin, M. (2013). Bioelectric signaling regulates head and organ size during planarian regeneration. *Development, 140*(2), 313-322. doi:10.1242/dev.086900

Besson, P., Driffort, V., Bon, E., Gradek, F., Chevalier, S., & Roger, S. (2015). How do voltage-gated sodium channels enhance migration and invasiveness in cancer cells? *Biochimica et Biophysica Acta, 1848*(10 Pt B), 2493-2501. doi:10.1016/j.bbamem.2015.04.013

Beyder, A., Rae, J. L., Bernard, C., Strege, P. R., Sachs, F., & Farrugia, G. (2010). Mechanosensitivity of Nav1.5, a voltage-sensitive sodium channel. *Journal of Physiology, 588*(Pt 24), 4969-4985. doi:10.1113/jphysiol.2010.199034

Black, J. A., Dib-Hajj, S., Cohen, S., Hinson, A. W., & Waxman, S. G. (1998). Glial cells have heart: rH1 Na+ channel mRNA and protein in spinal cord astrocytes. *Glia, 23*(3), 200-208. Retrieved from http://dx.doi.org/

Black, J. A., Liu, S., & Waxman, S. G. (2009). Sodium channel activity modulates multiple functions in microglia. *Glia, 57*(10), 1072-1081. doi:10.1002/glia.20830

Black, J. A., & Waxman, S. G. (2013). Noncanonical roles of voltage-gated sodium channels. *Neuron, 80*(2), 280-291. doi:10.1016/j.neuron.2013.09.012

Blackiston, D. J., McLaughlin, K. A., & Levin, M. (2009). Bioelectric controls of cell proliferation: ion channels, membrane voltage and the cell cycle. *Cell Cycle, 8*(21), 3519-3528. doi:9888 [pii]

Bourguignon, L. Y., Zhu, H., Shao, L., & Chen, Y. W. (2001). CD44 interaction with c-Src kinase promotes cortactin-mediated cytoskeleton function and hyaluronic acid-dependent ovarian tumor cell migration. *Journal of Biological Chemistry, 276*(10), 7327-7336. doi:10.1074/jbc.M006498200

Brackenbury, W. J. (2012). Voltage-gated sodium channels and metastatic disease. *Channels (Austin), 6*(5), 352-361. doi:10.4161/chan.21910

Brackenbury, W. J. (2016). Ion Channels in Cancer. In G. S. Pitt (Ed.), *Ion Channels in Health and Disease* (pp. 131-163): Elsevier Inc.

Brackenbury, W. J., Calhoun, J. D., Chen, C., Miyazaki, H., Nukina, N., Oyama, F., . . . Isom, L. L. (2010). Functional reciprocity between Na+ channel Nav1.6 and β1 subunits in the coordinated regulation of excitability and neurite outgrowth. *Proceedings of the National Academy of Sciences of the United States of America, 107*(5), 2283-2288. doi:10.1073/pnas.0909434107

Brackenbury, W. J., Chioni, A. M., Diss, J. K., & Djamgoz, M. B. (2007). The neonatal splice variant of Nav1.5 potentiates in vitro metastatic behaviour of MDA-MB-231 human breast cancer cells. *Breast Cancer Research and Treatment, 101*(2), 149-160. doi:10.1007/s10549-006-9281-1

Brackenbury, W. J., & Djamgoz, M. B. (2006). Activity-dependent regulation of voltage-gated $Na^+$ channel expression in Mat-LyLu rat prostate cancer cell line. *Journal of Physiology, 573*(Pt 2), 343-356. doi:10.1113/jphysiol.2006.106906

Brackenbury, W. J., & Isom, L. L. (2011). Na Channel beta Subunits: Overachievers of the Ion Channel Family. *Frontiers in Pharmacology, 2*, 53. doi:10.3389/fphar.2011.00053

Brackenbury, W. J., Yuan, Y., O'Malley, H. A., Parent, J. M., & Isom, L. L. (2013). Abnormal neuronal patterning occurs during early postnatal brain development of Scn1b-null mice and precedes hyperexcitability. *Proceedings of the National Academy of Sciences of the United States of America, 110*(3), 1089-1094. doi:10.1073/pnas.1208767110

Bravo-Cordero, J. J., Hodgson, L., & Condeelis, J. (2012). Directed Cell Invasion and Migration During Metastasis. *Current Opinion in Cell Biology, 24*(2), 277-283. doi:10.1016/j.ceb.2011.12.004
10.1016/j.ceb.2011.12.004.
Brisson, L., Driffort, V., Benoist, L., Poet, M., Counillon, L., Antelmi, E., . . . Roger, S. (2013). NaV1.5 Na(+) channels allosterically regulate the NHE-1 exchanger and promote the activity of breast cancer cell invadopodia. *Journal of Cell Science, 126*(Pt 21), 4835-4842. doi:10.1242/jcs.123901
Brisson, L., Gillet, L., Calaghan, S., Besson, P., Le Guennec, J. Y., Roger, S., & Gore, J. (2011). Na(V)1.5 enhances breast cancer cell invasiveness by increasing NHE1-dependent H(+) efflux in caveolae. *Oncogene, 30*(17), 2070-2076. doi:10.1038/onc.2010.574
Burridge, K., & Wennerberg, K. (2004). Rho and Rac take center stage. *Cell, 116*(2), 167-179. Retrieved from http://www.ncbi.nlm.nih.gov/pubmed/14744429
Campbell, T. M., Main, M. J., & Fitzgerald, E. M. (2013). Functional expression of the voltage-gated Na(+)-channel Nav1.7 is necessary for EGF-mediated invasion in human non-small cell lung cancer cells. *Journal of Cell Science, 126*(Pt 21), 4939-4949. doi:10.1242/jcs.130013
Carrithers, M. D., Chatterjee, G., Carrithers, L. M., Offoha, R., Iheagwara, U., Rahner, C., . . . Waxman, S. G. (2009). Regulation of podosome formation in macrophages by a novel splice variant of the sodium channel SCN8A. *Journal of Biological Chemistry, 284*(12), 8114-8126. doi:10.1074/jbc.M801892200
Carrithers, M. D., Dib-Hajj, S., Carrithers, L. M., Tokmoulina, G., Pypaert, M., Jonas, E. A., & Waxman, S. G. (2007). Expression of the voltage-gated sodium channel NaV1.5 in the macrophage late endosome regulates endosomal acidification. *Journal of Immunology, 178*(12), 7822-7832. doi:178/12/7822 [pii]
Catterall, W. A., Goldin, A. L., & Waxman, S. G. (2003). International Union of Pharmacology. XXXIX. Compendium of voltage-gated ion channels: sodium channels. *Pharmacological Reviews, 55*(4), 575-578. doi:10.1124/pr.55.4.7
Cervera, J., Alcaraz, A., & Mafe, S. (2016). Bioelectrical Signals and Ion Channels in the Modeling of Multicellular Patterns and Cancer Biophysics. *Scientific Reports, 6*, 20403. doi:10.1038/srep20403
Chen, B., Zhang, C., Wang, Z., Chen, Y., Xie, H., Li, S., . . . Chen, P. (2019). Mechanistic insights into Nav1.7-dependent regulation of rat prostate cancer cell invasiveness revealed by toxin probes and proteomic analysis. *FEBS Journal, 286*(13), 2549-2561. doi:10.1111/febs.14823
Chernet, B. T., Adams, D. S., Lobikin, M., & Levin, M. (2016). Use of genetically encoded, light-gated ion translocators to control tumorigenesis. *Oncotarget*. doi:10.18632/oncotarget.8036
Chernet, B. T., & Levin, M. (2014). Transmembrane voltage potential of somatic cells controls oncogene-mediated tumorigenesis at long-range. *Oncotarget, 5*(10), 3287-3306. Retrieved from http://dx.doi.org/
http://www.ncbi.nlm.nih.gov/pmc/articles/PMC4102810/pdf/oncotarget-05-3287.pdf
Chifflet, S., Correa, V., Nin, V., Justet, C., & Hernandez, J. A. (2004). Effect of membrane potential depolarization on the organization of the actin cytoskeleton of eye epithelia. The role of adherens junctions. *Experimental Eye Research, 79*(6), 769-777. doi:10.1016/j.exer.2004.08.031
Chifflet, S., Hernandez, J. A., & Grasso, S. (2005). A possible role for membrane depolarization in epithelial wound healing. *American Journal of Physiology: Cell Physiology, 288*(6), C1420-1430. doi:10.1152/ajpcell.00259.2004
Chifflet, S., Hernandez, J. A., Grasso, S., & Cirillo, A. (2003). Nonspecific depolarization of the plasma membrane potential induces cytoskeletal modifications of bovine corneal endothelial cells in culture. *Experimental Cell Research, 282*(1), 1-13. Retrieved from http://www.ncbi.nlm.nih.gov/pubmed/12490189

Cone, C. D., Jr. (1971). Maintenance of mitotic homeostasis in somatic cell populations. *Journal of Theoretical Biology, 30*(1), 183-194. Retrieved from http://www.ncbi.nlm.nih.gov/pubmed/5555270

Cone, C. D., Jr., & Cone, C. M. (1976). Induction of mitosis in mature neurons in central nervous system by sustained depolarization. *Science, 192*(4235), 155-158. Retrieved from http://www.ncbi.nlm.nih.gov/pubmed/56781

Contreras, G. F., Castillo, K., Enrique, N., Carrasquel-Ursulaez, W., Castillo, J. P., Milesi, V., . . . Latorre, R. (2013). A BK (Slo1) channel journey from molecule to physiology. *Channels (Austin), 7*(6), 442-458. doi:10.4161/chan.26242

Dang, I., Gorelik, R., Sousa-Blin, C., Derivery, E., Guerin, C., Linkner, J., . . . Gautreau, A. (2013). Inhibitory signalling to the Arp2/3 complex steers cell migration. *Nature, 503*(7475), 281-284. doi:10.1038/nature12611

Das, S., Yin, T., Yang, Q., Zhang, J., Wu, Y. I., & Yu, J. (2015). Single-molecule tracking of small GTPase Rac1 uncovers spatial regulation of membrane translocation and mechanism for polarized signaling. *Proceedings of the National Academy of Sciences of the United States of America, 112*(3), E267-276. doi:10.1073/pnas.1409667112

Djamgoz, M. B., & Onkal, R. (2013). Persistent current blockers of voltage-gated sodium channels: a clinical opportunity for controlling metastatic disease. *Recent Patents on Anti-Cancer Drug Discovery, 8*(1), 66-84. Retrieved from http://www.ncbi.nlm.nih.gov/pubmed/23116083

Driffort, V., Gillet, L., Bon, E., Marionneau-Lambot, S., Oullier, T., Joulin, V., . . . Roger, S. (2014). Ranolazine inhibits NaV1.5-mediated breast cancer cell invasiveness and lung colonization. *Molecular Cancer, 13*, 264. doi:10.1186/1476-4598-13-264

Ehrlich, J. S., Hansen, M. D., & Nelson, W. J. (2002). Spatio-Temporal Regulation of Rac1 Localization and Lamellipodia Dynamics during Epithelial Cell-Cell Adhesion. *Developmental Cell, 3*(2), 259-270. Retrieved from http://dx.doi.org/

Fairn, G. D., Schieber, N. L., Ariotti, N., Murphy, S., Kuerschner, L., Webb, R. I., . . . Parton, R. G. (2011). High-resolution mapping reveals topologically distinct cellular pools of phosphatidylserine. *Journal of Cell Biology, 194*(2), 257-275. doi:10.1083/jcb.201012028

10.1083/jcb.201012028.

Finkielstein, C. V., Overduin, M., & Capelluto, D. G. (2006). Cell migration and signaling specificity is determined by the phosphatidylserine recognition motif of Rac1. *Journal of Biological Chemistry, 281*(37), 27317-27326. doi:10.1074/jbc.M605560200

Fraser, S. P., Ding, Y., Liu, A., Foster, C. S., & Djamgoz, M. B. (1999). Tetrodotoxin suppresses morphological enhancement of the metastatic MAT-LyLu rat prostate cancer cell line. *Cell and Tissue Research, 295*(3), 505-512. Retrieved from http://www.ncbi.nlm.nih.gov/entrez/query.fcgi?cmd=Retrieve&db=PubMed&dopt=Citation&list_uids=10022970

Fraser, S. P., Diss, J. K., Chioni, A. M., Mycielska, M. E., Pan, H., Yamaci, R. F., . . . Djamgoz, M. B. (2005). Voltage-gated sodium channel expression and potentiation of human breast cancer metastasis. *Clinical Cancer Research, 11*(15), 5381-5389. doi:10.1158/1078-0432.CCR-05-0327

Fraser, S. P., Ozerlat-Gunduz, I., Brackenbury, W. J., Fitzgerald, E. M., Campbell, T. M., Coombes, R. C., & Djamgoz, M. B. (2014). Regulation of voltage-gated sodium channel expression in cancer: hormones, growth factors and auto-regulation. *Philosophical Transactions of the Royal Society of London. Series B: Biological Sciences, 369*(1638), 20130105. doi:10.1098/rstb.2013.0105

Friedl, P., Locker, J., Sahai, E., & Segall, J. E. (2012). Classifying collective cancer cell invasion. *Nature Cell Biology, 14*(8), 777-783. doi:10.1038/ncb2548

Fritz, R. D., Menshykau, D., Martin, K., Reimann, A., Pontelli, V., & Pertz, O. (2015). SrGAP2-Dependent Integration of Membrane Geometry and Slit-Robo-Repulsive Cues Regulates Fibroblast Contact Inhibition of Locomotion. *Developmental Cell, 35*(1), 78-92. doi:10.1016/j.devcel.2015.09.002

Garcia-Mata, R., Boulter, E., & Burridge, K. (2011). The 'invisible hand': regulation of RHO GTPases by RHOGDIs. *Nature Reviews: Molecular Cell Biology, 12*(8), 493-504. doi:10.1038/nrm3153
10.1038/nrm3153.
George, A. L., Jr. (2005). Inherited disorders of voltage-gated sodium channels. *Journal of Clinical Investigation, 115*(8), 1990-1999. Retrieved from http://www.ncbi.nlm.nih.gov/entrez/query.fcgi?cmd=Retrieve&db=PubMed&dopt=Citation&list_uids=16075039
Gillet, L., Roger, S., Besson, P., Lecaille, F., Gore, J., Bougnoux, P., . . . Le Guennec, J. Y. (2009). Voltage-gated Sodium Channel Activity Promotes Cysteine Cathepsin-dependent Invasiveness and Colony Growth of Human Cancer Cells. *Journal of Biological Chemistry, 284*(13), 8680-8691. doi:M806891200 [pii] 10.1074/jbc.M806891200
Grimes, J. A., Fraser, S. P., Stephens, G. J., Downing, J. E., Laniado, M. E., Foster, C. S., . . . Djamgoz, M. B. (1995). Differential expression of voltage-activated $Na^+$ currents in two prostatic tumour cell lines: contribution to invasiveness in vitro. *FEBS Letters, 369*(2-3), 290-294. Retrieved from http://www.ncbi.nlm.nih.gov/entrez/query.fcgi?cmd=Retrieve&db=PubMed&dopt=Citation&list_uids=7649275
Heo, W. D., Inoue, T., Park, W. S., Kim, M. L., Park, B. O., Wandless, T. J., & Meyer, T. (2006). PI(3,4,5)P3 and PI(4,5)P2 lipids target proteins with polybasic clusters to the plasma membrane. *Science, 314*(5804), 1458-1461. doi:10.1126/science.1134389
Hille, B. (1992). *Ionic channels of excitable membranes* (2nd ed.). Sunderland (Massachusetts): Sinauer Associates Inc.
House, C. D., Vaske, C. J., Schwartz, A., Obias, V., Frank, B., Luu, T., . . . Lee, N. H. (2010). Voltage-gated Na+ channel SCN5A is a key regulator of a gene transcriptional network that controls colon cancer invasion. *Cancer Research, 70*(17), 6957-6967. doi:10.1158/0008-5472.CAN-10-1169
House, C. D., Wang, B. D., Ceniccola, K., Williams, R., Simaan, M., Olender, J., . . . Lee, N. H. (2015). Voltage-gated Na+ Channel Activity Increases Colon Cancer Transcriptional Activity and Invasion Via Persistent MAPK Signaling. *Scientific Reports, 5*, 11541. doi:10.1038/srep11541
Kay, J. G., Koivusalo, M., Ma, X., Wohland, T., & Grinstein, S. (2012). Phosphatidylserine dynamics in cellular membranes. *Molecular Biology of the Cell, 23*(11), 2198-2212. doi:10.1091/mbc.E11-11-0936
Khaitan, D., Sankpal, U. T., Weksler, B., Meister, E. A., Romero, I. A., Couraud, P. O., & Ningaraj, N. S. (2009). Role of KCNMA1 gene in breast cancer invasion and metastasis to brain. *BMC Cancer, 9*, 258. doi:10.1186/1471-2407-9-258
Kraft, R., Krause, P., Jung, S., Basrai, D., Liebmann, L., Bolz, J., & Patt, S. (2003). BK channel openers inhibit migration of human glioma cells. *Pflügers Archiv. European Journal of Physiology, 446*(2), 248-255. doi:10.1007/s00424-003-1012-4
Krause, M., & Gautreau, A. (2014). Steering cell migration: lamellipodium dynamics and the regulation of directional persistence. *Nature Reviews: Molecular Cell Biology, 15*(9), 577-590. doi:10.1038/nrm3861
Lee, J. L., Wang, M. J., Sudhir, P. R., & Chen, J. Y. (2008). CD44 engagement promotes matrix-derived survival through the CD44-SRC-integrin axis in lipid rafts. *Molecular and Cellular Biology, 28*(18), 5710-5723. doi:10.1128/MCB.00186-08
Li, Q., Lau, A., Morris, T. J., Guo, L., Fordyce, C. B., & Stanley, E. F. (2004). A syntaxin 1, Galpha(o), and N-type calcium channel complex at a presynaptic nerve terminal: analysis by quantitative immunocolocalization. *Journal of Neuroscience, 24*(16), 4070-4081. doi:10.1523/JNEUROSCI.0346-04.2004
Lobikin, M., Chernet, B., Lobo, D., & Levin, M. (2012). Resting potential, oncogene-induced tumorigenesis, and metastasis: the bioelectric basis of cancer in vivo. *Physical Biology, 9*(6), 065002. doi:10.1088/1478-3975/9/6/065002

Lobikin, M., Lobo, D., Blackiston, D. J., Martyniuk, C. J., Tkachenko, E., & Levin, M. (2015). Serotonergic regulation of melanocyte conversion: A bioelectrically regulated network for stochastic all-or-none hyperpigmentation. *Sci Signal, 8*(397), ra99. doi:10.1126/scisignal.aac6609

Ma, Y. G., Liu, W. C., Dong, S., Du, C., Wang, X. J., Li, J. S., . . . Xie, M. J. (2012). Activation of BK(Ca) channels in zoledronic acid-induced apoptosis of MDA-MB-231 breast cancer cells. *PloS One, 7*(5), e37451. doi:10.1371/journal.pone.0037451

Machacek, M., Hodgson, L., Welch, C., Elliott, H., Pertz, O., Nalbant, P., . . . Danuser, G. (2009). Coordination of Rho GTPase activities during cell protrusion. *Nature, 461*(7260), 99-103. doi:10.1038/nature08242

Macmillan, S., Sheridan, R. D., Chilvers, E. R., & Patmore, L. (1995). A comparison of the effects of SCA40, NS 004 and NS 1619 on large conductance Ca(2+)-activated K+ channels in bovine tracheal smooth muscle cells in culture. *British Journal of Pharmacology, 116*(1), 1656-1660. Retrieved from http://dx.doi.org/

Magalhaes, M. A. O., & Glogauer, M. (2010). Pivotal Advance: Phospholipids determine net membrane surface charge resulting in differential localization of active Rac1 and Rac2. *Journal of Leukocyte Biology, 87*(4), 545-555. doi:10.1189/jlb.0609390

Manders, E. M. M., Verbeek, F. J., & Aten, J. A. (1993). Measurement of co-localization of objects in dual-colour confocal images. *Journal of Microscopy, 169*(3), 375-382. doi:10.1111/j.1365-2818.1993.tb03313.x

Marei, H., & Malliri, A. (2017). GEFs: Dual regulation of Rac1 signaling. *Small GTPases, 8*(2), 90-99. doi:10.1080/21541248.2016.1202635
10.1080/21541248.2016.1202635.

Marrison, J., Raty, L., Marriott, P., & O'Toole, P. (2013). Ptychography--a label free, high-contrast imaging technique for live cells using quantitative phase information. *Scientific Reports, 3*, 2369. doi:10.1038/srep02369

Martin, F., Ufodiama, C., Watt, I., Bland, M., & Brackenbury, W. J. (2015). Therapeutic value of voltage-gated sodium channel inhibitors in breast, colorectal and prostate cancer: a systematic review. *Frontiers in Pharmacology, 6*, 273. doi:10.3389/fphar.2015.00273

Masters, J. R., Thomson, J. A., Daly-Burns, B., Reid, Y. A., Dirks, W. G., Packer, P., . . . Debenham, P. G. (2001). Short tandem repeat profiling provides an international reference standard for human cell lines. *Proceedings of the National Academy of Sciences of the United States of America, 98*(14), 8012-8017. doi:10.1073/pnas.121616198

Moissoglu, K., Slepchenko, B. M., Meller, N., Horwitz, A. F., & Schwartz, M. A. (2006). In Vivo Dynamics of Rac-Membrane Interactions. *Molecular Biology of the Cell, 17*(6), 2770-2779. doi:10.1091/mbc.E06-01-0005

Nelson, M., Millican-Slater, R., Forrest, L. C., & Brackenbury, W. J. (2014). The sodium channel beta1 subunit mediates outgrowth of neurite-like processes on breast cancer cells and promotes tumour growth and metastasis. *International Journal of Cancer, 135*(10), 2338-2351. doi:10.1002/ijc.28890

Nelson, M., Yang, M., Dowle, A. A., Thomas, J. R., & Brackenbury, W. J. (2015). The sodium channel-blocking antiepileptic drug phenytoin inhibits breast tumour growth and metastasis. *Molecular Cancer, 14*(1), 13. doi:10.1186/s12943-014-0277-x

Nelson, M., Yang, M., Millican-Slater, R., & Brackenbury, W. J. (2015). Nav1.5 regulates breast tumor growth and metastatic dissemination in vivo. *Oncotarget, 6*(32), 32914-32929. doi:10.18632/oncotarget.5441

Nin, V., Hernandez, J. A., & Chifflet, S. (2009). Hyperpolarization of the plasma membrane potential provokes reorganization of the actin cytoskeleton and increases the stability of adherens junctions in bovine corneal endothelial cells in culture. *Cell Motility and the Cytoskeleton, 66*(12), 1087-1099. doi:10.1002/cm.20416

Pappalardo, L. W., Samad, O. A., Black, J. A., & Waxman, S. G. (2014). Voltage-gated sodium channel Nav 1.5 contributes to astrogliosis in an in vitro model of glial injury via reverse Na+ /Ca2+ exchange. *Glia, 62*(7), 1162-1175. doi:10.1002/glia.22671

Patel, F., & Brackenbury, W. J. (2015). Dual roles of voltage-gated sodium channels in development and cancer. *International Journal of Developmental Biology, 59*, 357-366. doi:10.1387/ijdb.150171wb

Persson, A. K., Estacion, M., Ahn, H., Liu, S., Stamboulian-Platel, S., Waxman, S. G., & Black, J. A. (2014). Contribution of sodium channels to lamellipodial protrusion and Rac1 and ERK1/2 activation in ATP-stimulated microglia. *Glia, 62*(12), 2080-2095. doi:10.1002/glia.22728

Pollard, T. D. (2007). Regulation of actin filament assembly by Arp2/3 complex and formins. *Annual Review of Biophysics and Biomolecular Structure, 36*, 451-477. doi:10.1146/annurev.biophys.35.040405.101936

Prevarskaya, N., Skryma, R., & Shuba, Y. (2018). Ion Channels in Cancer: Are Cancer Hallmarks Oncochannelopathies? *Physiological Reviews, 98*(2), 559-621. doi:10.1152/physrev.00044.2016

Remorino, A., De Beco, S., Cayrac, F., Di Federico, F., Cornilleau, G., Gautreau, A., . . . Coppey, M. (2017). Gradients of Rac1 Nanoclusters Support Spatial Patterns of Rac1 Signaling. *Cell Reports, 21*(7), 1922-1935. doi:10.1016/j.celrep.2017.10.069
10.1016/j.celrep.2017.10.069.

Ridley, A. J. (2011). Life at the leading edge. *Cell, 145*(7), 1012-1022. doi:10.1016/j.cell.2011.06.010
10.1016/j.cell.2011.06.010.

Ridley, A. J. (2015). Rho GTPase signalling in cell migration. *Current Opinion in Cell Biology, 36*, 103-112. doi:10.1016/j.ceb.2015.08.005
10.1016/j.ceb.2015.08.005. Epub 2015 Sep 10.

Roger, S., Besson, P., & Le Guennec, J. Y. (2003). Involvement of a novel fast inward sodium current in the invasion capacity of a breast cancer cell line. *Biochimica et Biophysica Acta, 1616*(2), 107-111. Retrieved from http://www.ncbi.nlm.nih.gov/pubmed/14561467
http://ac.els-cdn.com/S0005273603002347/1-s2.0-S0005273603002347-main.pdf?_tid=f2769a9e-edb1-11e4-8841-00000aacb35f&acdnat=1430231106_8706763e957edad5bf75ceae90f212df

Roger, S., Potier, M., Vandier, C., Le Guennec, J. Y., & Besson, P. (2004). Description and role in proliferation of iberiotoxin-sensitive currents in different human mammary epithelial normal and cancerous cells. *Biochimica et Biophysica Acta, 1667*(2), 190-199. doi:10.1016/j.bbamem.2004.10.002

Roger, S., Rollin, J., Barascu, A., Besson, P., Raynal, P. I., Iochmann, S., . . . Le Guennec, J. Y. (2007). Voltage-gated sodium channels potentiate the invasive capacities of human non-small-cell lung cancer cell lines. *International Journal of Biochemistry and Cell Biology, 39*(4), 774-786. doi:10.1016/j.biocel.2006.12.007

Sanguinetti, M. C., & Jurkiewicz, N. K. (1990). Two components of cardiac delayed rectifier K+ current. Differential sensitivity to block by class III antiarrhythmic agents. *Journal of General Physiology, 96*(1), 195-215. Retrieved from http://www.ncbi.nlm.nih.gov/pubmed/2170562

Sareen, D., Darjatmoko, S. R., Albert, D. M., & Polans, A. S. (2007). Mitochondria, calcium, and calpain are key mediators of resveratrol-induced apoptosis in breast cancer. *Molecular Pharmacology, 72*(6), 1466-1475. doi:10.1124/mol.107.039040

Schneider, C. A., Rasband, W. S., & Eliceiri, K. W. (2012). NIH Image to ImageJ: 25 years of image analysis. *Nature Methods, 9*(7), 671-675. Retrieved from http://www.ncbi.nlm.nih.gov/pubmed/22930834

Schwab, A., Fabian, A., Hanley, P. J., & Stock, C. (2012). Role of ion channels and transporters in cell migration. *Physiological Reviews, 92*(4), 1865-1913. doi:10.1152/physrev.00018.2011

Servitja, J. M., Marinissen, M. J., Sodhi, A., Bustelo, X. R., & Gutkind, J. S. (2003). Rac1 function is required for Src-induced transformation. Evidence of a role for Tiam1 and Vav2 in Rac activation by Src. *Journal of Biological Chemistry, 278*(36), 34339-34346. doi:10.1074/jbc.M302960200

Sontheimer, H., Fernandez-Marques, E., Ullrich, N., Pappas, C. A., & Waxman, S. G. (1994). Astrocyte Na+ channels are required for maintenance of Na+/K(+)-ATPase activity. *Journal of Neuroscience, 14*(5 Pt 1), 2464-2475. Retrieved from http://dx.doi.org/
http://www.jneurosci.org/content/jneuro/14/5/2464.full.pdf
Stock, C., & Schwab, A. (2015). Ion channels and transporters in metastasis. *Biochimica et Biophysica Acta (BBA) - Reviews in Biomembranes, 1848*(10 Pt B), 2638-2646. doi:10.1016/j.bbamem.2014.11.012
Stys, P. K., Sontheimer, H., Ransom, B. R., & Waxman, S. G. (1993). Noninactivating, tetrodotoxin-sensitive Na+ conductance in rat optic nerve axons. *Proceedings of the National Academy of Sciences of the United States of America, 90*(15), 6976-6980. Retrieved from http://dx.doi.org/
https://www.pnas.org/content/pnas/90/15/6976.full.pdf
Suman, R., Smith, G., Hazel, K. E., Kasprowicz, R., Coles, M., O'Toole, P., & Chawla, S. (2016). Label-free imaging to study phenotypic behavioural traits of cells in complex co-cultures. *Scientific Reports, 6*, 22032. doi:10.1038/srep22032
Sundelacruz, S., Levin, M., & Kaplan, D. L. (2008). Membrane potential controls adipogenic and osteogenic differentiation of mesenchymal stem cells. *PloS One, 3*(11), e3737. doi:10.1371/journal.pone.0003737
Sundelacruz, S., Levin, M., & Kaplan, D. L. (2009). Role of membrane potential in the regulation of cell proliferation and differentiation. *Stem Cell Rev, 5*(3), 231-246. doi:10.1007/s12015-009-9080-2
Szaszi, K., Sirokmany, G., Di Ciano-Oliveira, C., Rotstein, O. D., & Kapus, A. (2005). Depolarization induces Rho-Rho kinase-mediated myosin light chain phosphorylation in kidney tubular cells. *American Journal of Physiology: Cell Physiology, 289*(3), C673-685. doi:10.1152/ajpcell.00481.2004
Ulbricht, W. (1998). Effects of veratridine on sodium currents and fluxes. *Reviews of Physiology Biochemistry and Pharmacology, 133*, 1-54. Retrieved from http://www.ncbi.nlm.nih.gov/pubmed/9600010
Uphoff, C. C., Gignac, S. M., & Drexler, H. G. (1992). Mycoplasma contamination in human leukemia cell lines. I. Comparison of various detection methods. *Journal of Immunological Methods, 149*(1), 43-53. Retrieved from http://www.ncbi.nlm.nih.gov/pubmed/1374779
van Hennik, P. B., ten Klooster, J. P., Halstead, J. R., Voermans, C., Anthony, E. C., Divecha, N., & Hordijk, P. L. (2003). The C-terminal domain of Rac1 contains two motifs that control targeting and signaling specificity. *Journal of Biological Chemistry, 278*(40), 39166-39175. doi:10.1074/jbc.M307001200
Waheed, F., Speight, P., Kawai, G., Dan, Q., Kapus, A., & Szaszi, K. (2010). Extracellular signal-regulated kinase and GEF-H1 mediate depolarization-induced Rho activation and paracellular permeability increase. *American Journal of Physiology: Cell Physiology, 298*(6), C1376-1387. doi:10.1152/ajpcell.00408.2009
Winnicka, K., Bielawski, K., Bielawska, A., & Surazynski, A. (2008). Antiproliferative activity of derivatives of ouabain, digoxin and proscillaridin A in human MCF-7 and MDA-MB-231 breast cancer cells. *Biological & Pharmaceutical Bulletin, 31*(6), 1131-1140. Retrieved from http://www.ncbi.nlm.nih.gov/pubmed/18520043
Wu, Y. I., Frey, D., Lungu, O. I., Jaehrig, A., Schlichting, I., Kuhlman, B., & Hahn, K. M. (2009). A genetically encoded photoactivatable Rac controls the motility of living cells. *Nature, 461*(7260), 104-108. doi:10.1038/nature08241
Yang, M., & Brackenbury, W. J. (2013). Membrane potential and cancer progression. *Frontiers in Physiology, 4*, 185. doi:10.3389/fphys.2013.00185
Yang, M., Kozminski, D. J., Wold, L. A., Modak, R., Calhoun, J. D., Isom, L. L., & Brackenbury, W. J. (2012). Therapeutic potential for phenytoin: targeting Na(v)1.5 sodium channels to reduce migration and invasion in metastatic breast cancer. *Breast Cancer Research and Treatment, 134*(2), 603-615. doi:10.1007/s10549-012-2102-9

Yildirim, S., Altun, S., Gumushan, H., Patel, A., & Djamgoz, M. B. (2012). Voltage-gated sodium channel activity promotes prostate cancer metastasis in vivo. *Cancer Letters, 323*(1), 58-61. doi:10.1016/j.canlet.2012.03.036

Zhou, Y., Wong, C. O., Cho, K. J., van der Hoeven, D., Liang, H., Thakur, D. P., . . . Hancock, J. F. (2015). Membrane potential modulates plasma membrane phospholipid dynamics and K-Ras signaling. *Science, 349*(6250), 873-876. doi:10.1126/science.aaa5619

## Figure legends

**Figure 1.** $Na_v1.5$ is endogenously expressed in breast carcinoma cells and regulates the membrane potential. (A) MDA-MB-231 cells labeled with $Na_v1.5$ antibody (green), phalloidin to label the actin cytoskeleton (red), and DAPI to label the nucleus (blue). Insets show cell peripheries at higher magnification. (B) Typical whole-cell recording showing large transient and small persistent $Na^+$ current. The cell was depolarized to -10 mV for 50 ms following a 250 ms pre-pulse at -120 mV. (C) Expanded view of persistent $Na^+$ current 40-45 ms following onset of depolarization. (D) Activation and steady-state inactivation of $Na^+$ current. Normalized conductance ($G/G_{Max}$) was calculated from the current data and plotted as a function of voltage (n = 14). Normalized current ($I/I_{Max}$) was plotted as a function of the pre-pulse voltage (n = 9). Data are fitted with Boltzmann functions. (E) Expanded view of shaded area under activation and inactivation traces highlighting the window current. (F) Effect of $Na_v1.5$ shRNA knock-down on the $V_m$ compared to non-targeting shRNA control (n = 16). Data are mean and SEM. *P < 0.05; **P < 0.01; Student's t-test.

**Figure 2.** Tetrodotoxin hyperpolarizes, and veratridine depolarizes, the membrane potential. (A) Representative trace showing the inhibitory effect of tetrodotoxin (TTX; 30 μM) on $Na^+$ current, and recovery after washout. The cell was held at -120 mV for 250 ms before depolarizing to -10 mV for 50 ms. (B) Expanded view of persistent $Na^+$ current 40-45 ms following onset of depolarization. (C) Quantification of the normalized transient $Na^+$ current after TTX (30 μM) treatment and following washout (n = 7). (D) Quantification of the normalized persistent $Na^+$ current after TTX (30 μM) treatment and following washout (n = 4). (E) $V_m$ in control physiological saline solution, after TTX (30 μM) treatment and following washout. Solid line, mean; gray shading, SEM (n = 17). (F) Quantification of $V_m$ over the last 5 s in control, TTX, and washout (n = 17). (G) Representative trace showing effect of veratridine (100 μM) on $Na^+$ current. The cell was held at -120 mV for 250 ms before depolarizing to 0 mV for 50 ms. (H) Expanded view of persistent $Na^+$ current 40-45 ms

following onset of depolarization. (I) $V_m$ in control PSS and 120 s after perfusion with veratridine (n = 13). Data are mean and SEM. **P < 0.01; ***P < 0.001; repeated measures ANOVA with Tukey test for (C), (D), (F); Student's t test for (I).

**Figure 3.** Extracellular $Na^+$ sets the membrane potential and intracellular $Na^+$ level. (A) $V_m$ in control physiological saline solution, after extracellular $Na^+$ replacement with choline chloride and following washout. Solid line, mean; gray shading, SEM (n = 10). (B) Quantification of $V_m$ over the last 5 s in control, choline chloride, and washout (n = 10). (C) Representative SBFI fluorescence intensity (ratio of emission at 340 nm/380 nm) when cells were perfused with standard physiological saline (center panel), solution containing 10 mM $Na^+$ and 20 μM gramicidin (left panel) and solution containing 20 mM $Na^+$ and 20 μM gramicidin (right panel). Ratio images are color-coded so that warm and cold colors represent high and low $[Na^+]$, respectively. Scale bar = 10 μm. (D) Calibration of relationship between SBFI fluorescence intensity (340/380 ratio) and $[Na^+]_i$. Dashed line, linear regression ($r^2$ = 0.99; n = 40). (E) Quantification steady-state $[Na^+]_i$ in control physiological saline solution (n = 6), when extracellular $Na^+$ was replaced with NMDG (n = 3), and in TTX (30 μM; n = 3). (F) Effect of $Na_v1.5$ shRNA knock-down on $[Na^+]_i$ compared to non-targeting shRNA control (n = 3). Data are mean and SEM. *P < 0.05; **P < 0.01; ***P < 0.001; ANOVA with Tukey post hoc test for (A) and (E); Student's t test for (F).

**Figure 4.** The large conductance $Ca^{2+}$-activated $K^+$ channel $K_{Ca}1.1$ regulates the membrane potential but not intracellular $Na^+$. (A) MDA-MB-231 cells labeled with $K_{Ca}1.1$ antibody (green), phalloidin to label the actin cytoskeleton (red), and DAPI to label the nucleus (blue). (B) Western blot of $K_{Ca}1.1$ in control MDA-MB-231 cells and cells in which $Na_v1.5$ has been knocked down with shRNA. Positive control = rat brain lysate. Loading control = α-tubulin. (C) Representative perforated patch clamp recording showing activation of outward current using the $K_{Ca}1.1$ activator (NS-1619; 1 μM) and inhibition with iberiotoxin (100 nM). The cell

was held at -120 mV for 250 ms before depolarization to +60 mV for 300 ms. (D) Current-voltage relationship of the $K_{Ca}1.1$ current. Cells were held at -120 mV for 250 ms before depolarization to voltages ranging from -60 to +90 mV in 10 mV steps for 300 ms (n = 5). Data are fitted with single exponential functions. (E) Dose-dependent effect of NS-1619 on the steady-state $V_m$ (n ≥ 6). Data are fitted to a sigmoidal logistic function. (F) Effect of NS-1619 (1 μM) on steady-state $V_m$ (n = 12). (G) Effect of NS-1619 (1 μM, 5 min) on $[Na^+]_i$ (n = 22). (H) $V_m$ recorded using intracellular solution with free $[Ca^{2+}]$ buffered to 5.7 nM *vs.* 100 nM (n ≥ 10). Data are mean and SEM. **P < 0.01; Student's paired t-test.

**Figure 5.** $Na_v1.5$-dependent membrane potential depolarization regulates cell migration. (A) Representative scratch wounds at 0 h and 6 h into a wound healing assay ± TTX (30 μM) or NS-1619 (1 μM). Red dotted lines highlight wound edges. (B) Wound area during the migration assay ("gap remaining"), normalized to starting value (n = 3). (C) $t_{1/2}$ of wound closure (n ≥ 5). (D) Collective migration (μm/h) of cells closing the wound (n ≥ 5). (E) Instantaneous velocity (μm/s) of segmented cells (n ≥ 2662). (F) Polar histograms showing directionality of migrating cells at the leading edge of wounds (P <0.001; Friedman with Dunn's test). 90˚ = axis perpendicular to wound. Data in (B – D) are mean and SEM. Box plot whiskers in (E) show maximum and minimum values and horizontal lines show 75th, 50th, and 25th percentile values. *P < 0.05; **P < 0.01; ***P <0.001; ANOVA with Tukey test (C, D); Kruskal-Wallis with Dunn's test (E).

**Figure 6.** $Na_v1.5$-dependent membrane potential depolarization regulates lamellipodia formation. (A) Images of representative cells after treatment with TTX (30 μM) or NS-1619 (1 μM) for 3 h. Cells were fixed and stained with phalloidin (red) and DAPI (blue). Lower row shows masks of cells in the upper row, from which the circularity was calculated. (B) Circularity (n ≥ 61). (C) Feret's diameter (μm; n ≥ 57). (D) Number of MDA-MB-231 cells with

a lamellipodium (P < 0.001; $\chi^2$ test). Numbers in bars are %. Bars in (B) and (C) are mean and SEM. *P < 0.05; **P < 0.01; ***P < 0.001; ANOVA with Tukey test.

**Figure 7.** $Na_v1.5$ and $V_m$ regulate Rac1 activation/distribution. (A) Images of representative cells after treatment with TTX (30 μM) and NS-1619 (1 μM) for 3 h. Cells were labeled with Rac1-GTP antibody (green), phalloidin (red) and DAPI (blue). Arrows in the Rac1-GTP panels highlight the distribution or lack of expression at the leading edge. (B) Rac1-GTP signal density, measured across 20 arcs, in 0.43 μm radius increments, within a quadrant mask region of interest at the leading edge, normalized to the first arc (n ≥ 66). (C) Peak Rac1-GTP signal density per cell from (B), normalized to the first arc (n ≥ 66). (D) Total Rac1-GTP quantified in whole cell lysates using colorimetric small GTPase activation assay (n = 6). (E) Images of representative cells after treatment with TTX (30 μM) and NS-1619 (1 μM) for 3 h. Cells were labeled with Rac1-GTP antibody (green), total Rac1 antibody (red), and DAPI (blue). Arrows in the Rac1-GTP panels highlight the distribution or lack of expression at the leading edge. (F) Total Rac1 signal density, measured across 20 arcs, in 0.43 μm radius increments, within a quadrant mask region of interest at the leading edge, normalized to the first arc (n ≥ 59). (G) Peak Rac1 signal density per cell from (F), normalized to the first arc (n ≥ 59). (H) Ratio of Peak Rac1-GTP/Peak total Rac1 for each experimental repeat, normalized to control (n = 3). Data are mean and SEM. *P < 0.05; **P < 0.01; ***P < 0.001; ANOVA with Tukey test.

**Figure 8.** $Na_v1.5$ and $V_m$ regulate Rac1-GTP colocalization with phosphatidylserine. (A) Images of representative cells after treatment with TTX (30 μM) and NS-1619 (1 μM) for 3 h. Cells were labeled with Rac1-GTP antibody (green), annexin V (red) and DAPI (blue). Dashed lines highlight regions of interest at the leading edge. (B) Cytofluorogram showing colocalization of annexin V and Rac1-GTP staining in region of interest in control cell from (A), normalized to maximum in each channel. (C) Cytofluorogram showing colocalization of

annexin V and Rac1-GTP staining in region of interest in TTX cell from (A), normalized to maximum in each channel. (D) Cytofluorogram showing colocalization of annexin V and Rac1-GTP staining in region of interest in NS-1619 cell from (A), normalized to maximum in each channel. (E) Manders' corrected colocalization coefficients for annexin V and Rac1-GTP staining in regions of interest of cells after treatment with TTX (30 μM) and NS-1619 (1 μM) for 3 h (n = 30). (F) Li's intensity correlation quotient for Rac1-GTP and annexin V colocalization (n = 30). Data are mean and SEM. **P < 0.01; ***P < 0.001; ANOVA with Tukey test.

**Figure 9.** $Na_v1.5$ regulates Rac1 activation in live cells detected using a genetically encoded Rac1 FRET biosensor. (A) Images of representative cells after treatment ± TTX (30 μM) for 3 h. Rac1 activation biosensor distribution is shown in the donor (mTFP) channel. Images are color-coded so that warm and cold colors represent high and low values, respectively, for sensor distribution and activation (FRET). (B) Fluorescence intensity profile along line drawn across control cell in (A). (C) Fluorescence intensity profile along line drawn across TTX-treated cell in (A). (D) Emission ratio (FRET), for cells measured after treatment ± TTX (30 μM) for 3 h, normalized to control (n ≥ 33). Data are mean and SEM. **P < 0.01; Student's t test.

**Figure 10.** $Na_v1.5$-mediated morphological changes and migration are dependent on Rac1 activation. (A) Images of representative cells after treatment with TTX (30 μM) ± Rac1 inhibitor (EHT1864; 0.5 μM) for 3 h. Cells are labeled with CD44 antibody (red). (B) Circularity of cells after treatment with TTX (30 μM) ± EHT1864 (0.5 μM) for 3 h (n ≥ 308). (C) Feret's diameter (μm) of cells after treatment with TTX (30 μM) ± EHT1864 (0.5 μM) for 3 h (n ≥ 308). Data are mean and SEM. ***P < 0.001; ANOVA with Tukey test. (D) Proposed mechanism underlying $Na_v1.5$-mediated $V_m$-dependent morphological changes and migration. $Na_v1.5$ channels carry $Na^+$ influx, which depolarizes the $V_m$, causing redistribution of charged phosphatidylserine in the inner leaflet of the phospholipid bilayer, promoting

Rac1 redistribution and activation. Rac1 regulates cytoskeletal modification *via* the Arp2/3 complex and increasing phosphorylation of cortactin and cofilin, promoting acquisition of a promigratory phenotype (Pollard, 2007; Stock & Schwab, 2015). $Na^+$ influx through $Na_v1.5$ channels may also impact on migration and invasion through other mechanism(s), including via β1 subunit-dependent adhesion (Brisson et al., 2013; Carrie D House et al., 2010; C. D. House et al., 2015; Nelson et al., 2014).

Figure 1

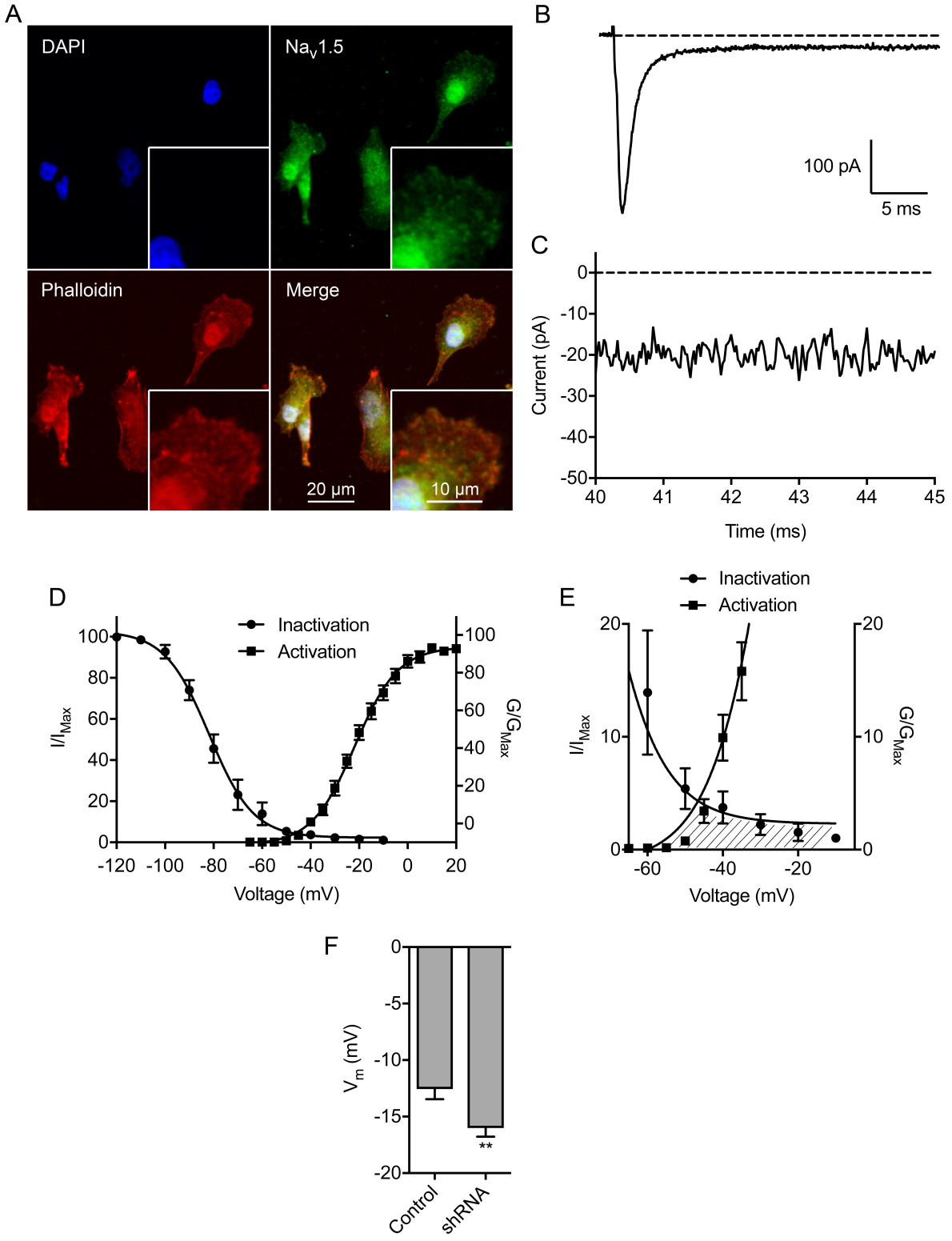
A
DAPI
Na$_V$1.5
Phalloidin
Merge
20 µm
10 µm
B
100 pA
5 ms
C
Current (pA)
0
-10
-20
-30
-40
-50
40
41
42
43
44
45
Time (ms)
D
Inactivation
Activation
I/I$_{Max}$
G/G$_{Max}$
100
80
60
40
20
0
-120
-100
-80
-60
-40
-20
0
20
Voltage (mV)
E
Inactivation
Activation
I/I$_{Max}$
G/G$_{Max}$
20
10
0
-60
-40
-20
Voltage (mV)
F
V$_m$ (mV)
0
-5
-10
-15
-20
**
Control
shRNA

Figure 2

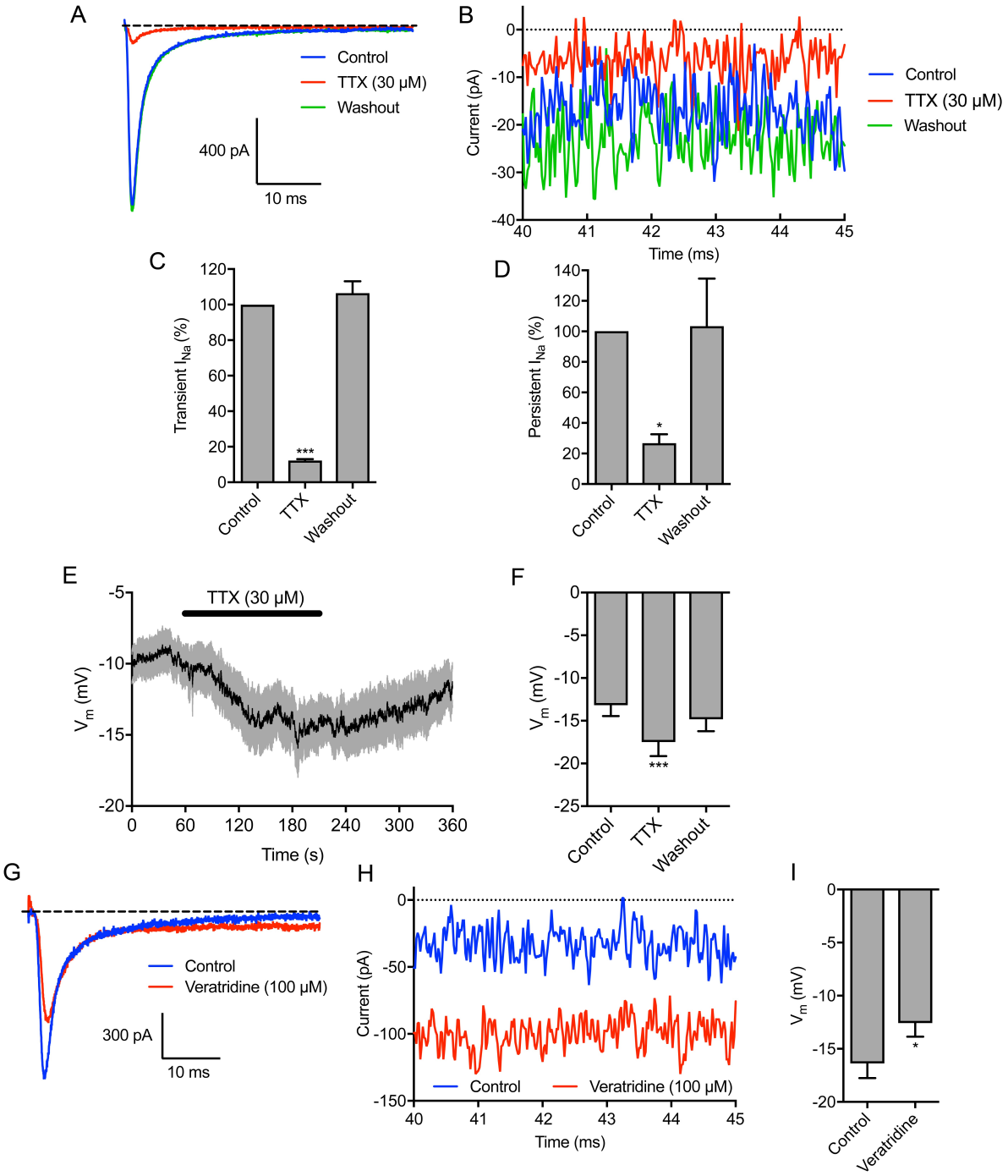
A
Control
TTX (30 μM)
Washout
400 pA
10 ms
B
Current (pA)
Time (ms)
Control
TTX (30 μM)
Washout
C
Transient $I_{Na}$ (%)
Control
TTX
Washout
D
Persistent $I_{Na}$ (%)
Control
TTX
Washout
E
TTX (30 μM)
$V_m$ (mV)
Time (s)
F
$V_m$ (mV)
Control
TTX
Washout
G
Control
Veratridine (100 μM)
300 pA
10 ms
H
Current (pA)
Control
Veratridine (100 μM)
Time (ms)
I
$V_m$ (mV)
Control
Veratridine

Figure 3

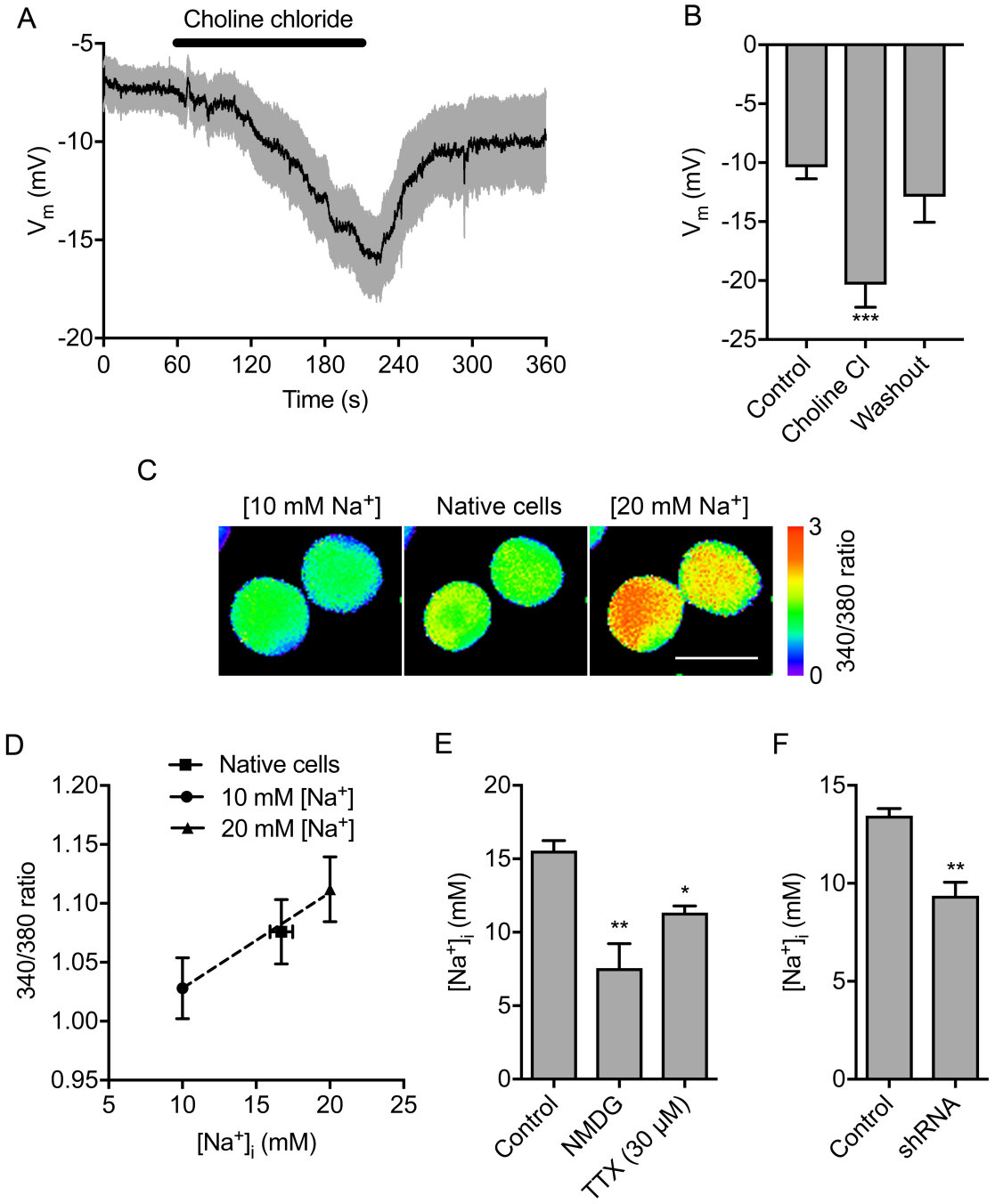
A
Choline chloride
$V_m$ (mV)
-5
-10
-15
-20
0
60
120
180
240
300
360
Time (s)
B
$V_m$ (mV)
0
-5
-10
-15
-20
-25
***
Control
Choline Cl
Washout
C
[10 mM Na+]
Native cells
[20 mM Na+]
3
0
340/380 ratio
D
Native cells
10 mM [Na+]
20 mM [Na+]
340/380 ratio
1.20
1.15
1.10
1.05
1.00
0.95
5
10
15
20
25
$[Na^+]_i$ (mM)
E
$[Na^+]_i$ (mM)
20
15
10
5
0
**
*
Control
NMDG
TTX (30 μM)
F
$[Na^+]_i$ (mM)
15
10
5
0
**
Control
shRNA

Figure 4

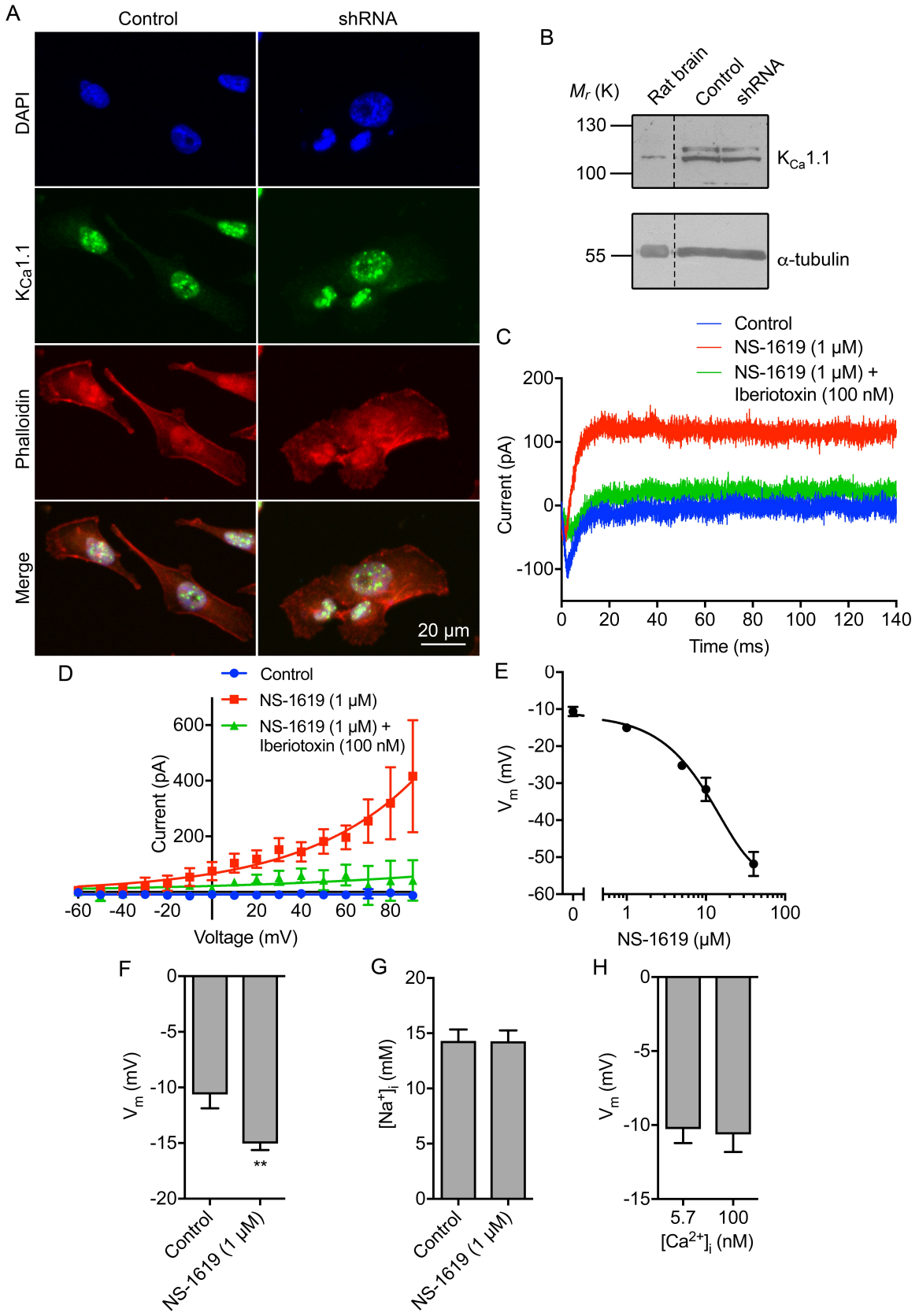
A
Control
shRNA
DAPI
KCa1.1
Phalloidin
Merge
20 µm
B
Mr (K)
Rat brain
Control
shRNA
130
100
KCa1.1
55
α-tubulin
C
Control
NS-1619 (1 µM)
NS-1619 (1 µM) +
Iberiotoxin (100 nM)
Current (pA)
Time (ms)
D
Control
NS-1619 (1 µM)
NS-1619 (1 µM) +
Iberiotoxin (100 nM)
Current (pA)
Voltage (mV)
E
Vm (mV)
NS-1619 (µM)
F
Vm (mV)
**
Control
NS-1619 (1 µM)
G
[Na+]i (mM)
Control
NS-1619 (1 µM)
H
Vm (mV)
5.7
100
[Ca2+]i (nM)

Figure 5

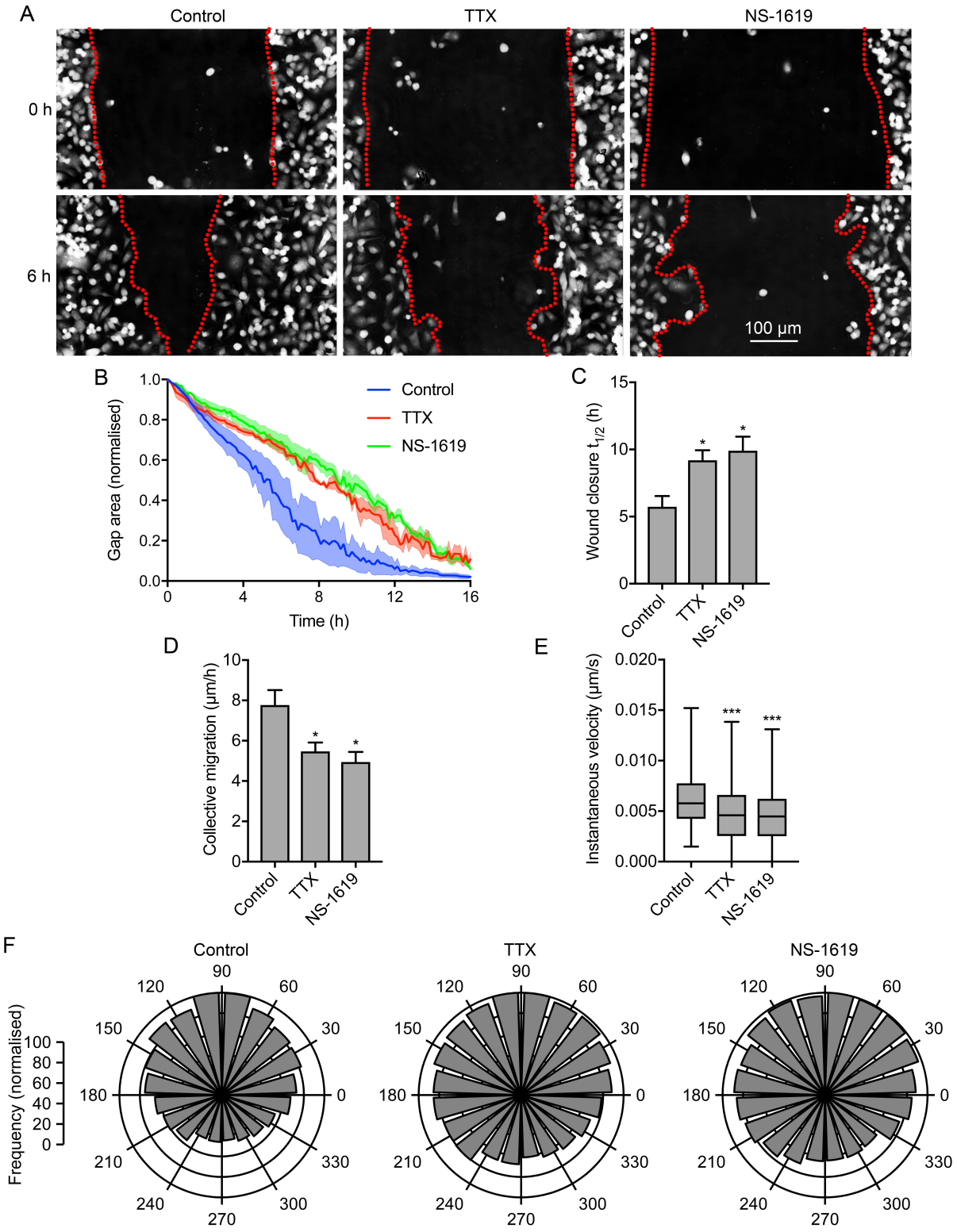
A
Control
TTX
NS-1619
0 h
6 h
100 µm
B
Gap area (normalised)
Time (h)
Control
TTX
NS-1619
C
Wound closure $t_{1/2}$ (h)
Control
TTX
NS-1619
D
Collective migration (µm/h)
Control
TTX
NS-1619
E
Instantaneous velocity (µm/s)
Control
TTX
NS-1619
F
Frequency (normalised)
Control
TTX
NS-1619

Figure 6

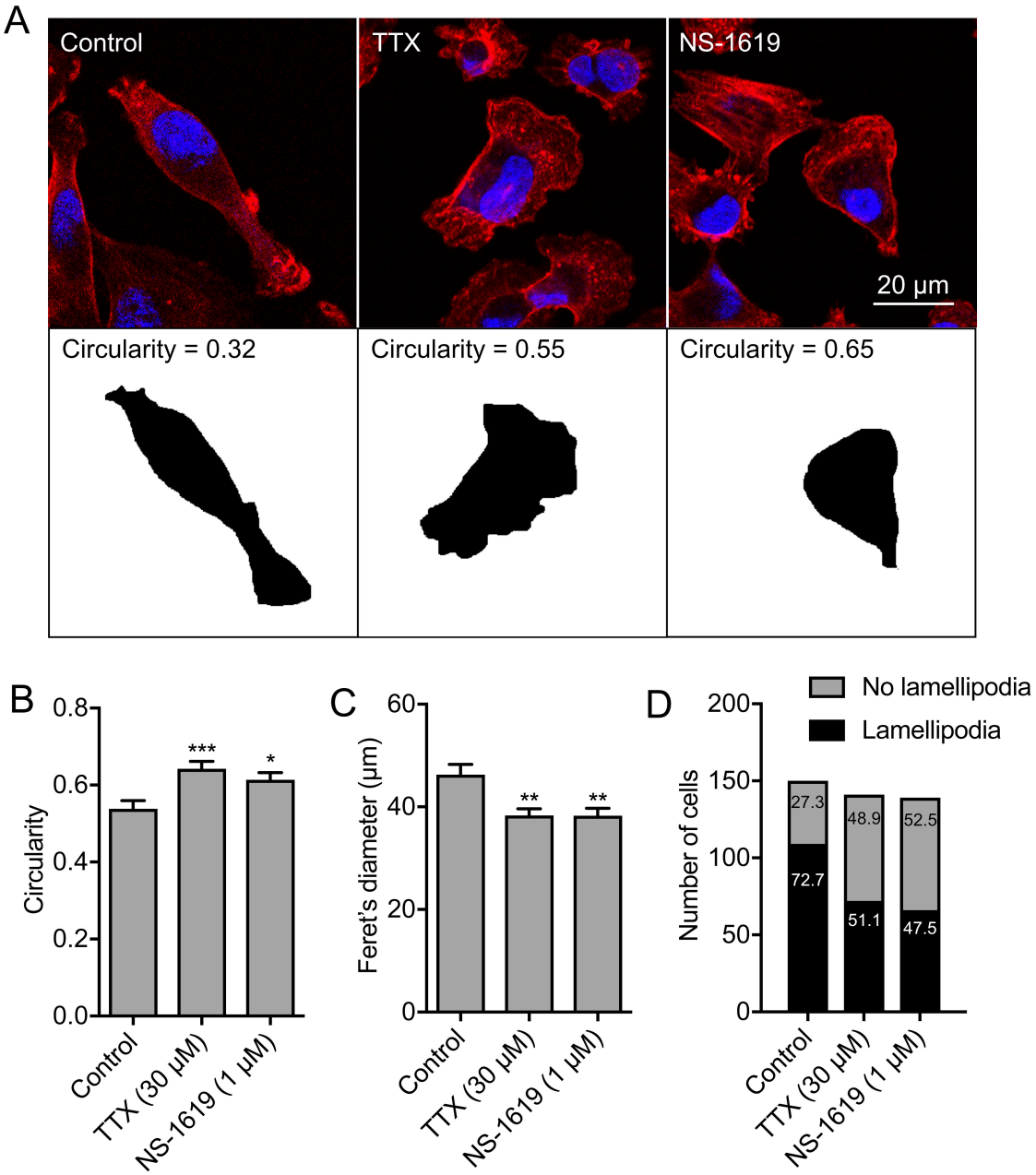
A
Control
TTX
NS-1619
20 µm
Circularity = 0.32
Circularity = 0.55
Circularity = 0.65
B
Circularity
0.8
0.6
0.4
0.2
0.0
***
*
Control
TTX (30 µM)
NS-1619 (1 µM)
C
Feret's diameter (µm)
60
40
20
0
**
**
Control
TTX (30 µM)
NS-1619 (1 µM)
D
No lamellipodia
Lamellipodia
Number of cells
200
150
100
50
0
27.3
72.7
48.9
51.1
52.5
47.5
Control
TTX (30 µM)
NS-1619 (1 µM)

Figure 7

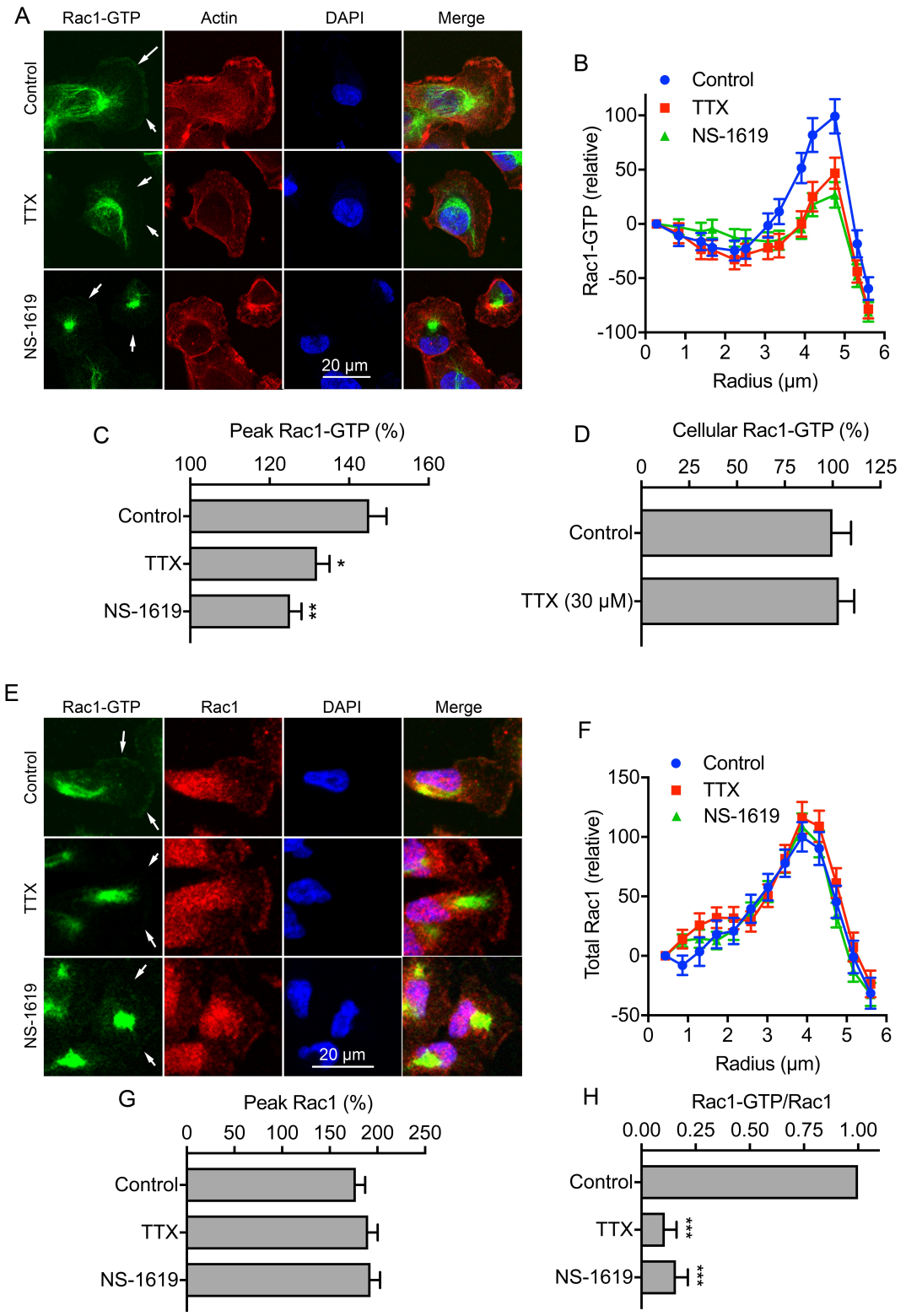
A
Rac1-GTP
Actin
DAPI
Merge
Control
TTX
NS-1619
20 µm
B
Control
TTX
NS-1619
Rac1-GTP (relative)
Radius (µm)
C
Peak Rac1-GTP (%)
Control
TTX
NS-1619
D
Cellular Rac1-GTP (%)
Control
TTX (30 µM)
E
Rac1-GTP
Rac1
DAPI
Merge
Control
TTX
NS-1619
20 µm
F
Control
TTX
NS-1619
Total Rac1 (relative)
Radius (µm)
G
Peak Rac1 (%)
Control
TTX
NS-1619
H
Rac1-GTP/Rac1
Control
TTX
NS-1619

Figure 8

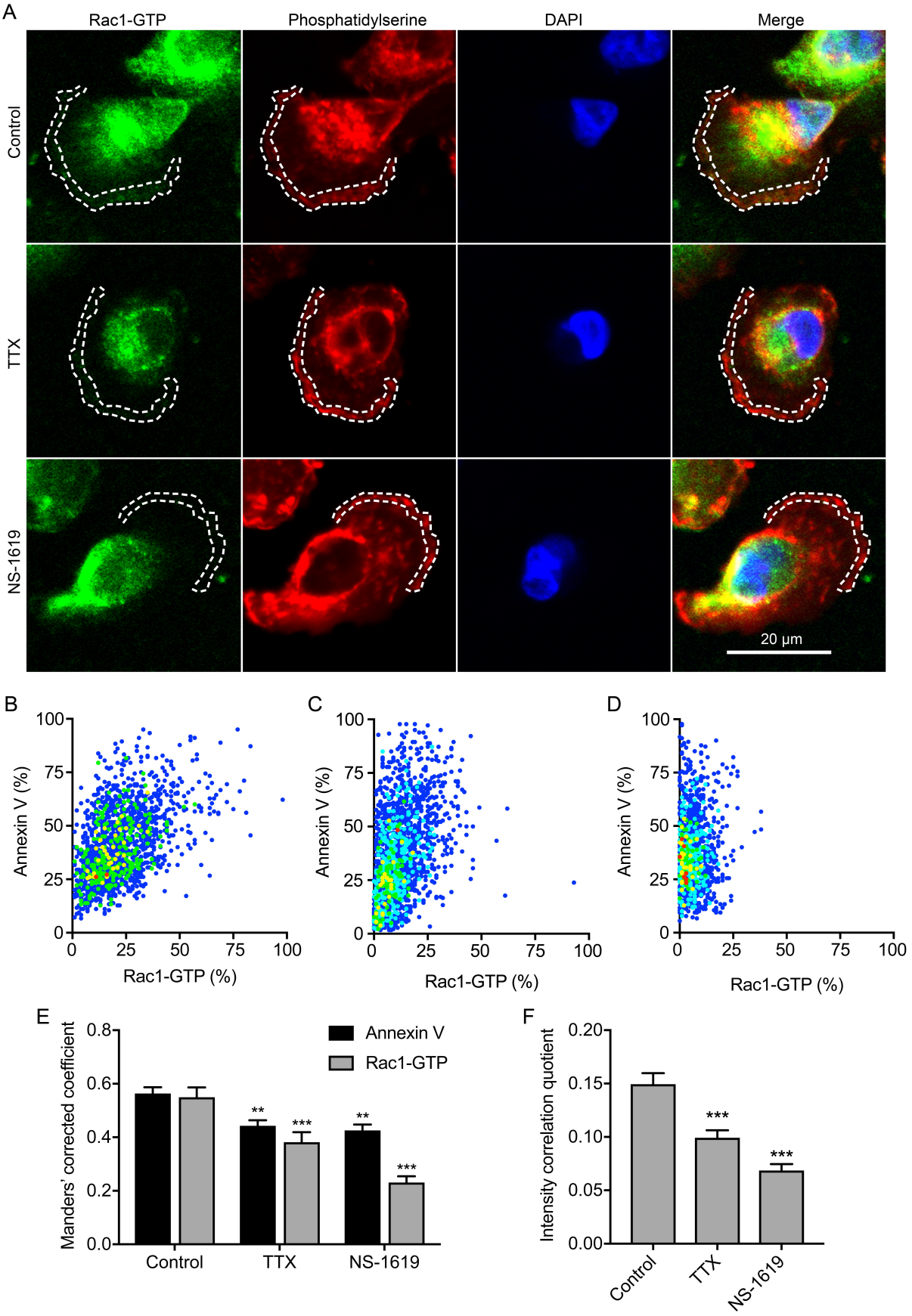
A
Rac1-GTP
Phosphatidylserine
DAPI
Merge
Control
TTX
NS-1619
20 µm
B
C
D
Annexin V (%)
Rac1-GTP (%)
E
Manders' corrected coefficient
Annexin V
Rac1-GTP
Control
TTX
NS-1619
F
Intensity correlation quotient

Figure 9

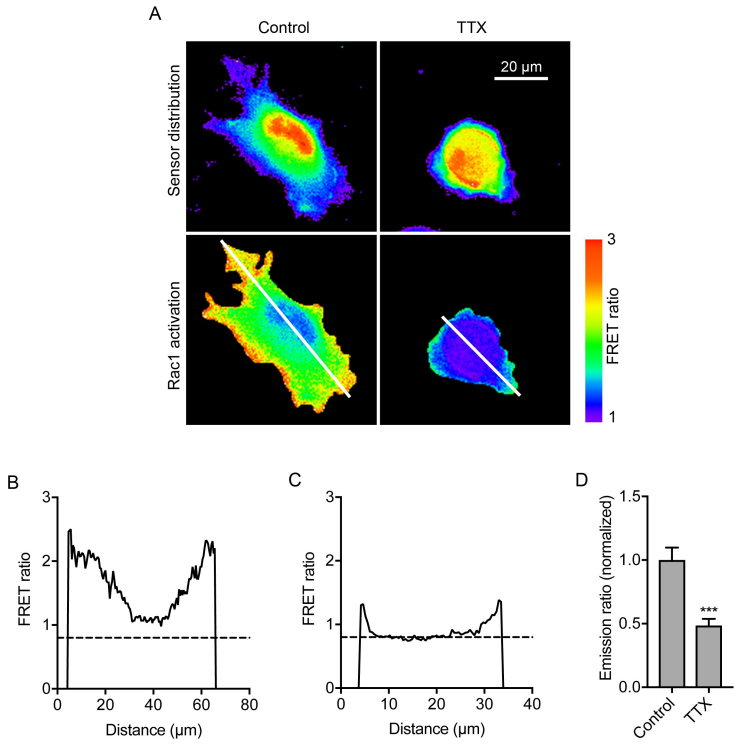
A
Control
TTX
20 µm
Sensor distribution
Rac1 activation
3
FRET ratio
1
B
FRET ratio
Distance (µm)
C
FRET ratio
Distance (µm)
D
Emission ratio (normalized)
***
Control
TTX

Figure 10

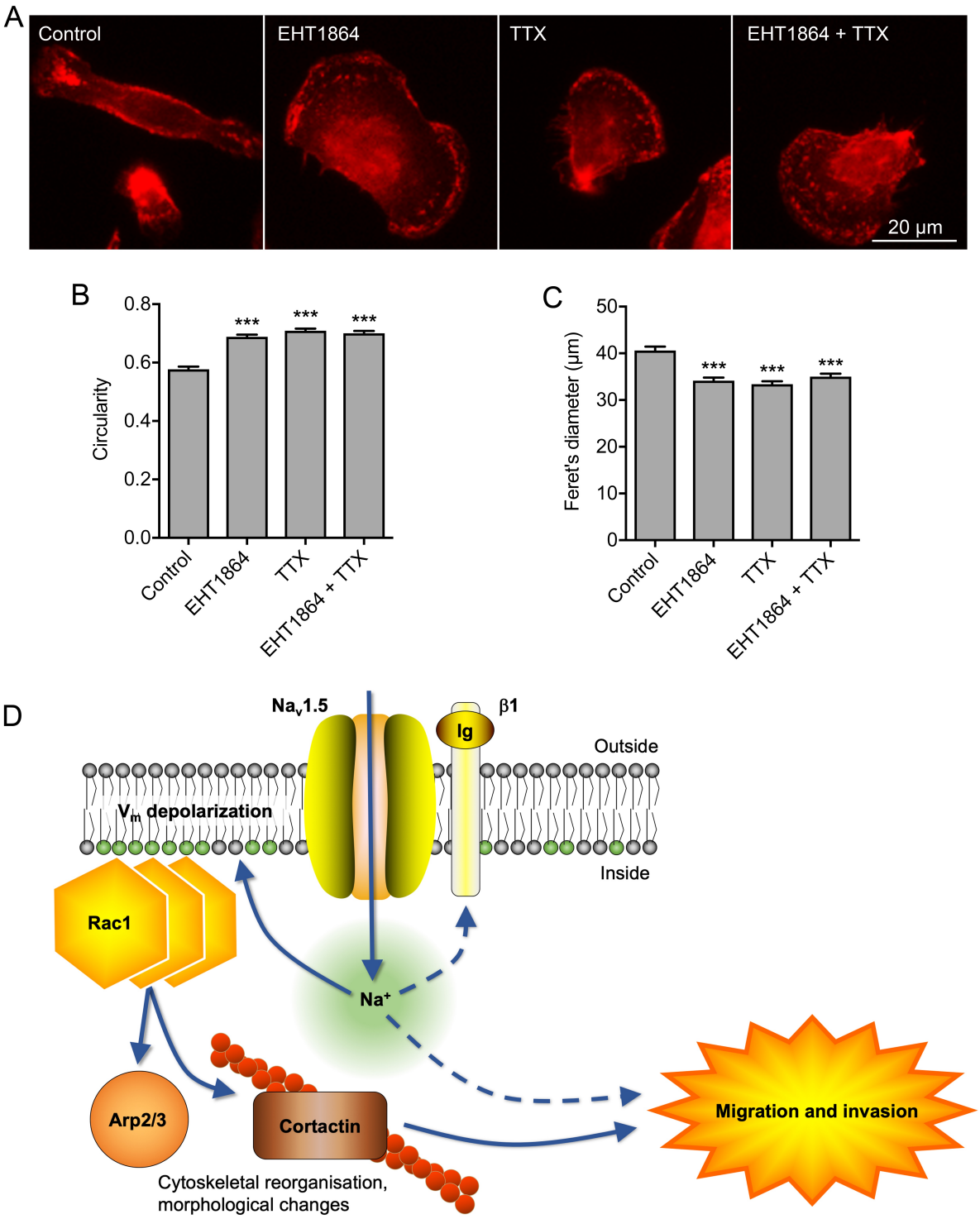
A
Control
EHT1864
TTX
EHT1864 + TTX
20 µm
B
Circularity
0.8
0.6
0.4
0.2
0.0
***
Control
EHT1864
TTX
EHT1864 + TTX
C
Feret's diameter (µm)
50
40
30
20
10
0
D
Nav1.5
β1
Ig
Outside
Inside
Vm depolarization
Rac1
Na+
Arp2/3
Cortactin
Cytoskeletal reorganisation,
morphological changes
Migration and invasion